The Thesis Committee for Keaton Munsterman
Certifies that this is the approved version of the following thesis:

Designing for Deck Stress Over Precast Panels In Negative Moment Regions

APPROVED BY
SUPERVISING COMMITTEE:

Supervisor:

Todd Helwig

Michael Engelhardt

Designing for Deck Stress Over Precast Panels In Negative Moment Regions

by

Keaton Munsterman

Thesis

Presented to the Faculty of the Graduate School of

The University of Texas at Austin

in Partial Fulfillment

of the Requirements

for the Degree of

Master of Science in Engineering

The University of Texas at Austin

December 2017

Dedication

To all my friends and family that have helped and encouraged me through this whole process.

Acknowledgements

I would like to thank the Texas Department of Transportation and their pursuit of research that financed this project. Specifically I would like to thank Bill Bunce, Chad Nutt, and Brandon Thompson for going over and beyond to help with each bridge. This project has proved to be worth far more than I expected, and I hope this research continues to benefit all of those involved.

I would also like to thank my professors who have guided this research process. Dr. Helwig, Dr. Engelhardt, and Dr. Bayrak have all been great teachers. Thank you for your insights and always being able to make a joke.

I would also like to thank Xiaomeng (George) Ge. You have been a great research partner and friend. I could not have done this without your help.

Finally, I would like to thank all of the staff and students at FSEL. Thank you for being so willing to help whenever needed, and always helping to make research an enjoyable experience.

Abstract

Designing for Deck Stress Over Precast Panels In Negative Moment Regions

Keaton Munsterman, M.S.E.

The University of Texas at Austin, 2017

Supervisor: Todd Helwig

One of the leading causes of structural deficiencies in the United States Bridge Inventory is related to deterioration and durability problems with concrete bridge decks (NCHRP 2004). The primary issue with bridge decks is related to cracking of the concrete that provides a direct conduit for moisture and other corrosion agents to permeate and attack the reinforcing steel. Adequate reinforcing steel is needed in the deck to minimize crack widths and therefore limit corrosion of reinforcing steel. A particular case of interest occurs when the bridge deck is constructed using partial-depth precast concrete deck panels (PCP) with cast-in-place (CIP) concrete topping. When this type of deck construction is used over the negative moment region of continuous steel or concrete girders, the amount of reinforcing steel that should be placed within the CIP concrete topping to provide adequate crack control is not currently well understood. This thesis is part of a larger study being conducted for the Texas Department of Transportation that is examining this issue.

In the study reported in this thesis, two newly constructed bridges were instrumented to monitor the behavior of the bridge deck. These bridges did not use continuous girders, but rather had simply supported prestressed concrete girders, with a bridge deck constructed using a "poor-boy" construction joint detail over interior bents. Each bridge utilized three different reinforcement layouts centered over an interior bent within the poor-boy joint detail. Strain gages in each portion provided constant readings to display the distribution of strain across the bridge deck. Each bridge was monitored over a period from when the deck was cast until when the bridge was opened to traffic. Live load tests were also conducted to provide data on strains induced by heavy trucks.

Based on the field data, no clear correlation was found between the amount of steel added and the strain measured. However, based on the measured data combined with field observations of cracking, the current standard reinforcement appears to be adequate in controlling the crack widths for the poor-boy deck detail. While the poor-boy deck joint detail is different from deck details used over negative moment regions of continuous girders, this data provides useful insights in to bridge deck behavior that will help guide future phases of the larger study.

Table of Contents

List of Tables

List of Figures

Chapter 1: Introduction

1.1 INTRODUCTION

One of the leading causes of structural deficiencies in the United States Bridge Inventory is related to deterioration and durability problems with concrete bridge decks (NCHRP 2004). The primary issue with bridge decks is related to cracking of the concrete that provides a direct conduit for moisture and other corrosion agents to permeate and attack the reinforcing steel. The region of the bridge that is the most susceptible to cracking is the area around interior supports of continuous girder systems where bending moments lead to tension in the top of the composite girders. While cracking in the concrete is unavoidable, the sizes of the cracks can be controlled by providing well-detailed reinforcing steel. Cracking can result from a number of sources including stresses resulting from the applied loading or volumetric changes in the concrete. Volumetric changes are a function of the age of the concrete. The age of the concrete that is used for the decking is often complicated by the forming systems that is employed during deck construction. Many bridge decks are constructed using partial-depth precast concrete deck panels (PCPs) in which the forming panel is approximately half of the total design deck thickness. The PCPs are typically precast in a prestressing yard and then shipped to the job site.

The Texas Department of Transportation (TxDOT) first utilized PCP formwork beginning in 1963. The PCP have created durable concrete bridge decks as well as reducing construction costs compared to full depth cast-in-place bridge decks. Chase and Laman (1999) estimated that Texas spends $1 billion annually in maintenance and repair of existing bridges. To facilitate both the design and construction of bridges, TxDOT

often utilizes standard details for commonly used components. The TxDOT standard reinforcing detail for the PCP bridge decks was recently changed with a reduction in the total amount of steel. While TxDOT commonly uses "poor-boy" continuous construction in which a continuous deck is used on simply supported prestressed concrete girders, the state is beginning to make use of continuous prestressed girder systems. However there are a number of questions regarding the required steel in the interior support regions. These questions arise since the American Association of State Highway and Transportation Officials (AASHTO) bridge design specifications (2014) does not provide clear guidance on the amount of deck steel when PCP formwork is utilized.

To investigate the behavior of the concrete bridge decks with PCP forms at the interior support regions, TxDOT funded a research project to study the behavior. The investigation includes field monitoring, laboratory studies, and parametric finite element analytical studies. This thesis documents the initial results from the field monitoring. The remainder of this chapter provides an overview of the applicable design provisions and TxDOT reinforcing standards as well as an overview of the scope of the research investigation and this thesis.

1.2 AASHTO GUIDELINES

The AASHTO Bridge Design Specifications (2014) provide two methods for the design of concrete bridge decks: Empirical Design Method and Traditional Design Method. The Empirical Design Method is based upon previous research focusing on the combined use of arching action and flexural strength of the deck and reinforcing steel. Despite its derivation from research testing, AASHTO precludes the use of the Empirical Design Method when the deck is not fully cast-in-place, such as in the case of the partial depth PCP system that is commonly used in Texas. The Traditional Design Method is not

precluded from use in the PCP system and utilizes conventional modeling of force transfer through the flexural behavior of the panel. This method assumes four layers of steel in the section (two layers of both longitudinal and transverse reinforcing), and includes the reinforcement in the panel as primary reinforcing.

1.3 CURRENT DESIGN PROVISIONS

In 2014, TxDOT implemented a new standard detail for bridge deck reinforcing based on research that reduces the amount of reinforcing while maintaining strength and durability (Holt and Smith, 2014). Figure 1.1 shows a comparison of the old detail versus the new detail. In addition to controlling cracking for long-term durability, the new detail provides adequate strength for wheel loads as well as extreme loads applied to guardrails and. A transition from the guidelines of the Standard Design Method to the Empirical Design Method addresses the unnecessary design capacity under normal serviceability by reducing the top mat reinforcing from #4 @ 9 in. longitudinal steel and #5 @ 6 in. transverse steel to #4 @ 9 in. in both directions. With the reduction in reinforcing in the overall bridge deck, the overhangs include supplemental #5 @ 9 in. spacing to ensure adequate strength for vehicle impact loads. The 40% reduction in steel still exceeds the Empirical Design Method minimum amount of steel required by AASHTO by 50%.

The detail also recognizes the benefits of the steel location in controlling cracking, and has changed the order of the steel so that the longitudinal steel is placed above the transverse steel. This provides better crack control for transverse cracks perpendicular to the girders.

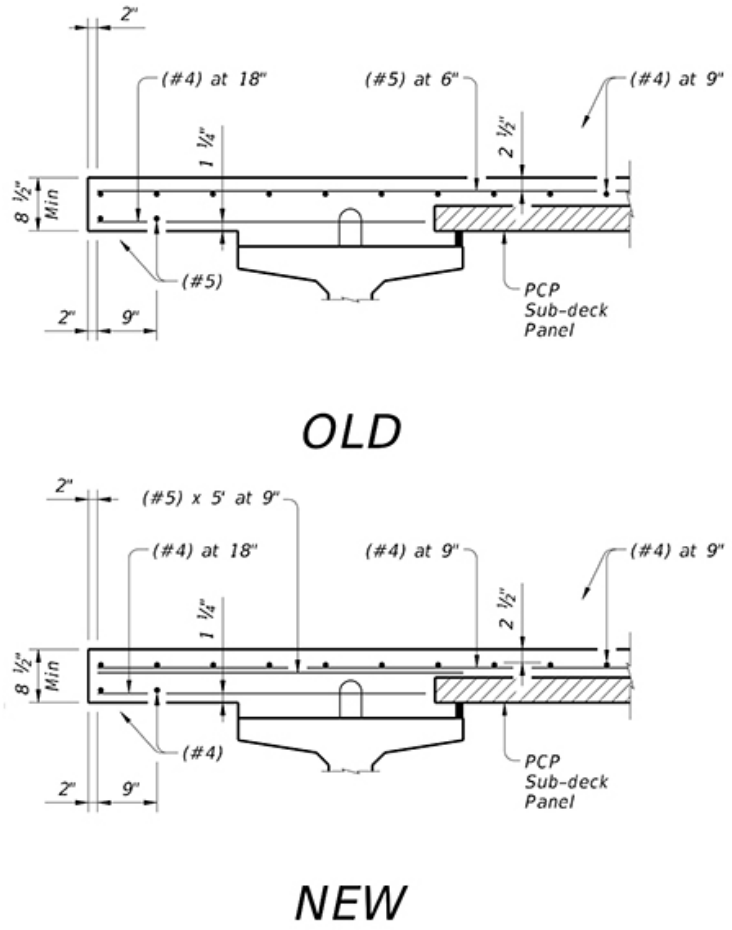

Figure 1.1: TxDOT Deck Reinforcing Detail (Holt and Smith, 2014)

1.4 SCOPE OF RESEARCH STUDY

Most concrete bridges in the Texas consist of simply supported prestressed girders with "poor boy" continuous decks that are essentially a "jointless" deck. The behavior or reinforcing requirements in concrete bridge systems with truly continuous girders are not well understood. A research study was funded at the University of Texas to investigate the behavior of concrete decks around the interior supports of continuous girder systems with partial-depth PCPs for the deck forming. The study includes field monitoring, laboratory tests, and parametric finite element analyses. Although Texas is

beginning to design spliced prestressed concrete girders, most concrete girder systems in the past have been the simply supported girders with the "poor-boy" continuous (jointless) deck. Due to the limited number of continuous prestressed concrete girders in Texas, the initial focus of the field monitoring was on simply supported girders with the poor-boy continuous deck. The field monitoring focused on the behavior of newly-constructed bridges so that the volumetric changes that occur early in the life of the bridge deck could be captured. The instrumented bridges were then subjected to truck loading to gain a measure of the behavior of the bridge deck with known live-loading conditions. The deck reinforcing details were varied within the bridges to get an indication of the impact on deck cracking. This thesis focuses on field data from the initial instrumentation efforts that included two bridges. The next section of this introductory chapter provides an overview of the layout of the thesis.

1.5 CHAPTER ORGANIZATION

This thesis has been divided into five chapters. Following this introductory chapter, Chapter 2 provides an overview of previous work and background information such as the use of PCPs in bridge construction, deck reinforcing, and deck cracking. Chapter 3 provides an overview of the instrumentation configuration and bridge geometries of the instrumented bridges in the first phase of the investigation. A presentation and discussion of the data that was collected on two bridges is provided in Chapter 4. Finally, Chapter 5 provides a summary of the findings and recommendations of the thesis.

Chapter 2: Background

2.1 INTRODUCTION

This chapter provides an overview of the necessary background information and summary of past studies pertinent to the research discussed in the thesis. The background information and previous studies will begin focusing on partial depth precast concrete deck panels (PCPs) frequently used in Texas followed by a discussion on the cracking behavior of concrete bridge decks. Verification of the monitoring instrumentation is presented to provide guidelines for the installation and assurance of reliability of the vibrating wire strain gages used on the research investigation that is the focus of the thesis. Finally, an overview of crack width formulations and criteria to assess deck cracking that are used in the field studies for this investigation is provided. For the purposes of discussion, the term "negative moment" is used in this chapter referring to bending moments that cause tension in the top of the concrete deck.

2.2 BACKGROUND OF DECK PANELS

There has been an extensive amount of research carried out on the use partial-depth precast concrete panels for form work for bridge decks used in Texas since their introduction in 1963. One of the first major studies carried out on PCPs was reported by Buth, et al. in 1972. The investigation included laboratory testing on the panels subjected to 2 million cyclic applications of a simulated design axle load to a bridge deck as well as static loads to failure. While some cracking was noted on the surface of the deck during the tests, no distress was observed at the interface between the PCP and the cast-in-place (CIP) concrete. For the purposes of discussion, the application of the CIP concrete on top of the PCP to form the entire bridge deck will be referred to as the "topping slab".

Following the tests in Texas, the Illinois department of transportation evaluated the performance of PCPs, permanent metal deck forms (PMDF), and wood forms (Barker (1975)). With regard to PCPs, the extent of impact of different surface finishes as well as some panels with shear reinforcing bars extending into the topping slab were studied. It was found that no shear reinforcement was necessary at the panel-to-topping slab interface to achieve adequate bond.

There have been a number of recent studies that have focused on the development of full depth panels for accelerated bridge construction as well as precast forms that extend over the fascia girder to form the overhangs. Many of these systems were made of grout pockets such as the precast overhang system studied by Mander and Head (2010) and Ley et al. (2010). Although a full depth panel has attractive features for speed of construction, many of these systems are not suitable to accommodate the wide range of bridge geometries that occur in practice. In as such, conventional partial-depth PCPs such as those used throughout Texas bridges and in this project, will likely be the predominant forming systems for many years to come.

Figure 2.1 shows a series of pictures that demonstrate the configuration of the PCPs and the support conditions in the field. Figure 2.1a shows that PCPs in the state that they are often delivered to the field. Most PCPs are prestressed in the direction that spans between adjacent girders. Approximately 3-4 inches of the prestressing strand protrudes from the panels as can be seen in Figure 2.1a. The girders are typically erected as shown in Figure 2.1b, after which the PCPs are installed along the length.

Deck panels minimize the construction time by their ability to be placed quickly and reduce the volume of concrete to be cast-in-place on the bridge. To accommodate differential camber and other geometrical issues in the field, the panels are supported on a dense foam bedding strip that can be adjusted easily and require minimal anchorage.

Figure 2.1c shows the bedding strip installed on the girders supporting the PCP. The bedding strip material can be cut to the required thickness to position a given concrete panel to the proper elevation. In most instances, the bedding strip height is typically in the range of 0.5" thick to 4 inches thick. After the PCPs have been fully installed, the transverse and longitudinal deck reinforcing is added to the bridge as shown in Figure 2.1d. The bridge in Figure 2.1d had a support skew of approximately 45 degrees and the TxDOT detail in this condition utilizes permanent metal deck forms (PMDF) around the support region. In bridges with normal supports, the PCPs will be provided all the way up to the support region with no PMDF utilized.

(a) PCP on Site *(b) Girders before PCP*

Figure 2.1 continued next page

(c) PCP Bedding Strip *(d) Top Layer Reinforcement in Place*

Figure 2.1 (a) - (d) PCP Details

Additional details are defined in Chapter 3 for the construction process.

2.3 PROPERTIES OF DECK PANELS

Furr, et al. (1970) conducted a series of laboratory studies and field verification of the composite action between the panel and CIP portion. Multiple strength and cyclic tests have also been completed verifying the panels to be stronger and stiffer than the conventional full depth CIP deck. For design, the panels can be considered a part of the structural deck system, and are to be considered fully composite in the bottom half of the deck. Since the primary strength direction for the panels is considered to be perpendicular to the supporting girders, the panels are reinforced with pre-tensioned strands in the transverse direction, and mildly reinforced in the longitudinal direction. Culmo (2009) describes, in the transverse direction, the slab can be idealized like a multi-span continuous flexural element. Although the partial depth PCPs only span between adjacent girders, moments causing "tension" in the top of the deck from the idealized continuous flexural element occur directly over the tops of the girders. The deck

reinforcing that is added over the top of the PCPs controls cracking. Full composite action between the panels and the topping concrete is achieved without the use of special detailing, such as horizontal shear connectors.

Graddy, Burns and Klingner (1995) summarized experimental testing programs that studied the behavior of the panels under both static and cyclic loads. The work also included analytical investigations that provided insight into factors affecting the design thickness of bridge slabs. Their findings showed the bridge deck thickness should be based on the provisions for isotropically reinforced deck using the empirical design method and also evaluated the punching shear capacity of the deck. Under typical truck loads, punching shear is not expected to be a controlling failure, but future increases in truck loads and traffic may make this limit state more important. In addition, the reserve capacity of the compression membrane of the panel is recommended to be included in punching shear and flexural design.

For many years and up until relatively recent times, the panels were not used near the ends of bridges. Instead a thickened cast-in-place deck was used near the expansion joints using either removable plywood forms or PMDF as shown previously in Figure 2.1(d). Coselli (2004) conducted research looking at the behavior of systems where the panels were extended to the expansion joint and found good behavior was achieved without the thickened end regions. However, one concern with extending the panels to the end of the bridge was the long-term fatigue behavior of the deck panels. Agnew (2007) conducted fatigue tests on PCP panels and considered the impact of both positive and negative moment. Similar to the early versions of the PCPs that were studied and reported on by Buth et al. (1972), Agnew found that the panels did not have a problem with fatigue or delamination between the panel and the topping slab under cyclic loads.

Following up on some of the work mentioned above by Buth et al. (1972) and Barker, delamination between the PCP and the topping slab may be a concern with regard to durability of the bridge decks. However, Dowell and Smith (2006) carried out tests on panels with a variety of bond-surface finishes and found no problems with delamination occurring. Of note is the potential for delamination between the PCP and CIP concrete due to the larger shear stresses present in the deck. TxDOT has had some isolated cases where signs of delamination were exhibited; however, these problems can likely be attributed to either isolated cases of material issues with the PCP or some other contamination of the PCP/CIP joint.

2.4 UTILIZING PCP-CIP DECK AT SPECIFIC LOCATION

One of the first studies utilizing PCPs in the negative moment region was carried out and reported by Tsui, et al. (1986). The study included full-scale experiments on a composite pre-stressed concrete girder system where half the deck was constructed with PCPs and the other half had a cast-in-place (CIP) deck. The negative moment experiments showed that the deck cast with PCPs was stronger, stiffer, and more crack resistant than the CIP deck.

Coselli and Bayrak et al. (2006) evaluated the performance of bridge slab behavior at expansion joints under increased design loads with the following variables:

- girders with normal supports and girders with a 45° support skew,
- girder spacings of 8 ft. and 10 ft.,
- full depth cast-in-place bridge deck (I-Beam Thickened Slab and Uniform Thickness Slab End) and 4 in. PCP and 4 in. CIP on topping slab (similar to that used in this project).

The results showed that 1) the adhesion at the interface between PCP and CIP concrete topping was sufficient for the section to act as a unit; 2) Cracks due to restrained shrinkage are inevitable in bridge decks using PCP. Although, the results showed that shrinkage cracking has no detrimental effect on capacity and performance, recommendations were made for further investigation to develop procedures to reduce cracking and to improve the durability and service life of the deck.

2.5 REINFORCEMENT IN THE CAST-IN-PLACE LAYER

Foster (2010) and Kwon (2012) focused on the behavior of "Texas Poor Boy Joints" and design recommendation on reducing top mat reinforcement in bridge decks. The Texas Poor Boy Joint consists of simply supported girders with a continuous concrete deck over the "interior" support region. The report focused on effectively reducing the amount of steel in the CIP portion of the slab and control cracking in the PCPs. The work by Foster and Kwon concluded that the longitudinal reinforcing should not be reduced, retaining the reinforcing layout of #4 @ 9" in the longitudinal direction, but the #5 @ 6" transverse steel may be able to be reduced to #4 @ 6" or D20 @ 6" in the transverse direction.

As noted in the introductory section, there is currently a disconnect in the reinforcing steel detailing requirements in the AASHTO LRFD Specification for continuous steel and pre-stressed concrete girders that utilize PCP panels. While there is some guidance suggested for the continuous steel girder applications, vague exceptions to the specification requirements are given in the Commentary. The AASHTO Specification however does not provide guidance for the case of continuous pre-stressed concrete girders, and precludes the use of the Empirical Design Method when utilizing PCP.

Research conducted at Iowa State University (Phares et al., 2015), focused on steel detailing requirements on continuous pre-stressed concrete girder bridge with respect to the termination point for reinforcing steel. The study considered the recommendations given in the AASHTO Specification versus practices required by the Iowa Department of Transportation (IDOT). The findings from field studies and finite element modeling suggested that an increase in the area of steel as well as increasing the length for development had minimal effects on reducing the strain. In the field studies, transverse cracks that were observed over the pier and around the locations at approximatley1/8 of the span length were concluded to be mainly due to secondary moments induced by deck shrinkage. Another observation was that bridges with larger skew angles have lower strains over the intermediate supports. Secondary moments may be benefiting the negative moment performance as they may counteract the live load negative moment. The benefit may be significant enough that limited tensile stresses in the deck may occur leading to minimal to no deck cracking. The research study also suggested that the negative moment over the pier may not be significantly affected by the geometries of the bridge.

Besides the research summarized above regarding PCP-CIP bridge deck, with the support from TxDOT, Mander, et al (2012) investigated different types of continuity connection details used for continuous concrete girder bridges across the United States that allow span lengths beyond 150 ft., which was inspired for the negative-moment zone bridge deck project. Different splice connection details, such as On-Pier Splicing with Continuity Diaphragms and In-Span Splicing with Cantilevered Pier Segments, have been proposed with advantages and disadvantages of each approach and with an emphasis on constructability and long-term serviceability. While all systems have their

merits, a mixed solution is perhaps the most desirable and should be considered, specifically a partially pre-stressed solution.

2.6 SHRINKAGE

There are many factors that can affect the strain in concrete. The study discussed in this thesis is directed at two primary factors, creep and shrinkage. Collins and Mitchell (1997) define creep as the increase in strain as a stress is held constant. Without specific tests, it is difficult to accurately estimate the amount of creep deformation. A linear approximation can be used to calculate the strain after the initial loading using the applied stress over a period of time t.

$$\varepsilon_{cf}(\mathrm{t}, t_i) = \left({f_{ci}}/{E_{c,eff}}\right) \qquad \textbf{2.1}$$

$$E_{c,eff} = \left({E_{ci}}/{1 + \Phi(t, t_i)}\right) \qquad \textbf{2.2}$$

Shrinkage is the change in strain due to moisture levels changing causing expansion and contractions. The rate of shrinkage is highly dependent on the composition of the mix. Aggregate type and water content are key components to the shrinkage rate. For moist-cured concrete,

$$\varepsilon_{sh} = -k_s k_h \left({t}/{35 + t}\right) 0.51 * 10^{-3} \qquad \textbf{2.3}$$

t= time in days exposed to drying

k_s = Size factor

k_h = Humidity factor

2.7 CRACK WIDTH PREDICTION

The prediction of crack widths varies significantly based on the methods that are based upon empirical data and force distribution models. DeStefano, et al (2003) compared a theoretical cracked model to several solutions including Gergely-Lutz's cracking equation in ACI, the Kaar-Mattock expression, the current AASHTO simplified standard, and the proposed AASHTO equation while accounting for the difference between exposure condition and applications.

Recommendations on the acceptable crack widths range from 0.004 to 0.008 in. for corrosive conditions and 0.008 to 0.012 in. for non-corrosive conditions (Broms, 1965 and Krauss & Rogalla, 1996). ACI 224-01 uses a guide of crack width under service loads and exposure conditions to be 0.016 in. for dry air, 0.012 in. for humid and moist air, and 0.007 in. for deicing chemicals.

The limit of cracks should be as such that it does not hinder the serviceability or durability of the structure. CEB-FIP (1990) uses the basic crack width prediction formula to estimate the crack widths over a given length of section.

$$w_k = l_{s,max}(\varepsilon_{sm} - \varepsilon_{cm} - \varepsilon_{cs}) \quad \textbf{2.4}$$

$l_{s,max}$ = Length over which slip between steel and concrete occurs

ε_{sm} = Average steel strain within $l_{s,max}$

ε_{cm} = Average concrete strain within $l_{s,max}$

ε_{cs} = Strain of concrete due to shrinkage

Single cracks are created by exceeding the tensile strain limit of the concrete. Strain is then transferred through the reinforcing steel across the crack to the concrete on either side. For a crack pattern to stabilize, the strain in the concrete and steel must be

equal at a point between cracks at least twice the transmission length apart. The transmission length is the distance over which slip occurs between the concrete and steel. Strains for calculating single cracks and stabilized cracks can then be calculated using this formula to determine the crack spacing and average strains. The concrete surrounding the tension reinforcing, known as the effective area of concrete in tension $A_{c,eff}$ (Figure 2.2), is typically the start of the cracks and located at the end of the transfer length of steel. This effective area considers the non-uniform stress distribution where the stresses are transmitted through the transfer of bond forces between the steel and concrete. Using the distribution of forces through the effective area, crack widths can be calculated for that region. Cracking can also be due to imposed deformations where the steel strain is increased in a similar proportion of the deformation.

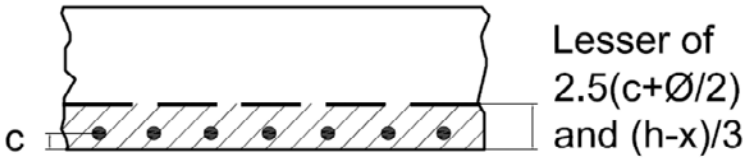

Figure 2.2: Concrete Slab Effective Area in Tension

Comparative tests have shown that better behavior results from using more small bars close together rather than large bars far apart to control the crack widths. Controlling crack widths plays a large role due to the longevity of a structure as well as maintaining an aesthetic structure. In the 1960's, the following equation was developed based on results from experiments (Gergely-Lutz 1968):

$$w_c = 0.000076\beta f_s \sqrt[3]{d_c A} \qquad \textbf{2.5}$$

where:

w_c = crack width, in.

β = factor relating the strain at the tension face to the strain at the centroid of the reinforcement

f_s = stress in steel reinforcement, (ksi)

d_c = distance from tension face to centroid of nearest reinforcement layer, in.

A = average effective concrete area per bar of the flexural tension reinforcement, in^2. (For a single layer of reinforcement of constant spacing, the term A simplifies to 2 d_c*s)

s = reinforce bar spacing, in.

Similar to the Gergely-Lutz equation, another crack width formula was developed at approximately the same time and is known as the Kaar-Mattock (1962) equation. This prediction model is based on a statistical analysis of experimental data.

$$w_c = 0.000115\beta f_s \sqrt[4]{A} \qquad \textbf{2.6}$$

The variables in this expression have been previously define.

When the Gergely-Lutz equation was adopted by AASHTO, simplifications were made to some of the variables. Crack width and the β factor were combined into a Z factor that depends on the exposure conditions. Assumptions were made that the crack limit is 0.016-in and the β factor was averaged to 1.2 resulting in the following expression:

$$f_{sa} = \frac{Z}{\sqrt[3]{d_c A}} \leq 0.6 f_y \qquad \textbf{2.7}$$

where,

f_{sa} = allowable reinforcement stress (ksi)

Z = 170 for moderate exposure conditions

= 130 for severe exposure conditions

= 100 for precast box culverts

= 155/ β for cast-in-place box culverts

Problems associated with the above equations have been raised in that increased concrete cover intensifies the cracking problem, which is not the behavior that has been observed in practice. To avoid issues with the expression, although a larger cover may be provided, AASHTO allows designers to limit the clear cover to 2 in. for calculations. This limit manipulation raises questions regarding the validity and accuracy of the equation. Other problems come from difficulty finding the effective concrete area (A) when there are multiple layers and sizes of reinforcing.

Frosch (1999, 2001) created a crack equation based on theoretical derivations rather than empirical testing. His model is based on relating strain in the reinforcing to the crack spacing, and the crack spacing correlates to the amount of concrete cover d*. His model produces similar predictions to the Gergely-Lutz and Kaar-Mattock equations.

$$s = 2\sqrt{\left(\left(\frac{w_c E_s}{2 f_s \beta}\right)^2 - d_c^2\right)} \qquad \textbf{2.8}$$

$$w_c = 2\, {f_s}/{E_s}\, \beta \sqrt{(d_c^2 + ({s}/{2})^2)} \qquad \textbf{2.9}$$

where:

w_c = crack width, in.

f_s = stress in steel reinforcement (ksi)

β = factor relating the strain at the tension face to the strain at the centroid of the reinforcement

d_c = distance from tension face to centroid of nearest reinforcement layer, in.

s = reinforce bar spacing (in.)

And the crack spacing is not larger than d* =$\sqrt{d_c^2 + (0.5s)^2)}$

Based on recommendations from Frosch, in 1999 ACI 318 adopted the following expression:

$$s = \frac{540}{f_s} - 2.5c_c \leq \frac{432}{f_s} \qquad \textbf{2.10}$$

where,

c_c = clear concrete cover on reinforcement nearest the tension face, in.;

w_c = 0.016 in. limiting crack width.;

$d_c = c_c + 0.5$ in., (i.e., #8 average bar size.);

$\beta = 1 + 0.08\ d_c$;

with the other variables as defined previously.

The new AASHTO LRFD proposed equation is

$$f_{sa} = \frac{700\gamma_e\gamma_r}{\beta(s + 2d_c)} \leq .8f_y \qquad \textbf{2.11}$$

where,

f_{sa} = allowable service level stress in the reinforcement, ksi;

γ_e = exposure factor,

= 1.0 for Case 1,

= 0.75 for Case 2;

γ_r = reinforcement factor,

= 0.75 for smooth weld-wire fabric,

= 1.00 for all other types of reinforcement;

$$\beta = 1 + {}^{d_c}/_{0.7(h - d_c)} \qquad \textbf{2.12}$$

with the remaining variables as defined previously.

The proposed AASHTO equation is essentially the same as the ACI 318 equation with the following modifications: The limiting crack width is approximately 0.017 in., which is slightly larger than the value of 0.016 in. used previously; The addition of an exposure factor, γ_e, is included to maintain a distinction between different environmental conditions; The addition of a reinforcement factor, γ_r, to recognize the fact that research suggests smooth welded-wire fabric has reduced bond properties, most notably for wider wire spacing, compared to other reinforcement types.

The equation is written in terms of allowable stress to be consistent with past practice, although rearranging the equation to be written in terms of maximum permitted bar spacing, s, can be done easily;

The β-factor is made an integral part of the equation rather than an assumed "average" value;

The d_c term is retained in the formal development of the cracking model instead of using the clear cover with an assumed "average" rebar size of #8

The β factor is a linear interpolation of crack width at the outer most face of steel to the tension face of the concrete.

The expression for Z factor given in the current AASHTO LRFD specifications is:

$$Z = {}^{155}/_{\beta}, \text{ where } \beta = 1 + {}^{d_c}/_{0.7d} \qquad \textbf{2.13}$$

The amount of concrete cover plays a significant role for the crack width interpolation. The 2 in. limit on the cover in the calculations that was discussed earlier is also a reasonable limit since most flexural members do not exceed this value for the concrete cover. DeStefano, et al (2003) remarks that the inclusion of factors accounting

for exposure condition have been a topic of debate. An area's normal conditions may be extremely different given the region. Case 1 and Case 2 are proposed instead of the "normal" and "severe" to distinguish regional areas and components on the bridge that are subject to more stringent crack control. The proposed limit typically stays slightly less conservative for Case 2 compared to the cracking model. The ACI equation remains the least conservative since it does not factor in an exposure condition. The current AASHTO equation changes drastically between minimally conservative for low stress and highly conservative as the 0.6 F_y limit is approached.

2.8 SUMMARY

The information presented in this chapter establishes a good background discussion of previous studies for the work discussed in the remainder of the thesis related to the behavior of bridges with PCP. This will help to give guidelines for instrumentation and analysis of the field monitoring. This testing will lead to improving the TxDOT reinforcing details and increase the durability of the bridge decks.

Chapter 3: Field instrumentation

3.1 OVERVIEW

Field measurements have been used in many studies and proven essential to gathering data for improving the understanding of the both the structural and material behavior trends of concrete. This chapter introduces the equipment used for instrumentation, and outlines the process of assessing, instrumenting, and monitoring the selected bridges during construction. Vibrating Wire Gages (VWG) with data logging equipment were the primary tools for data measurements and collection. The data that is presented in this study was taken from two bridges with different geometries; however a similar layout of the gages were used to study the variations in behavior. The length of time for monitoring was selected to ensure adequate data was collected demonstrating the fundamental behavior. The data that was gathered from these studies provides valuable insight into potential lab testing as well as validation data for analytical models.

3.2 INSTRUMENTATION EQUIPMENT

The primary objective of this project is to get an accurate representation of the behavior of the early stages in the life of the bridge. The focus of the project objective is directed to the negative moment region over interior bents. These moment regions vary depending on the type of bridge and the method of construction. To capture the strains induced in the concrete due to volumetric changes, VWG's were continuously monitored during the early life of the concrete following casting of the bridge deck. The data gathered provides insight into the fundamental behavior of the freshly cast concrete as well as validation data for finite element models of the bridge deck.

3.3 VIBRATING WIRE GAGE

The most sensitive component of the setup is the VWG. In past studies (Yousefpour (2015)), the Geokon Vibrating Wire Gage Model 4200, shown in Figure 3.1, has proven a reliable, mechanical gage that measures strain using the natural frequency of a tensioned steel wire subjected to deformations. The schematic of the gage shows the principle components that consist of the gage itself and a magnetic plucker used to excite the gage. The primary component of the gage consists of a tensioned steel wire and two anchorage end blocks. The magnetic plucker excites the tensioned wire and the frequency of vibration is monitored. Variations in the fundamental frequency are then correlated with changes in mechanical strain. The thermistor also provides valuable data related to the temperature at the gage location. The whole configuration is delivered from the manufacturer with each portion ready for installation. When being installed, the two pieces were secured to each other in the field by an adjustable hose clamp to prevent separation during placement and vibration of the concrete. The gage configuration is as described below.

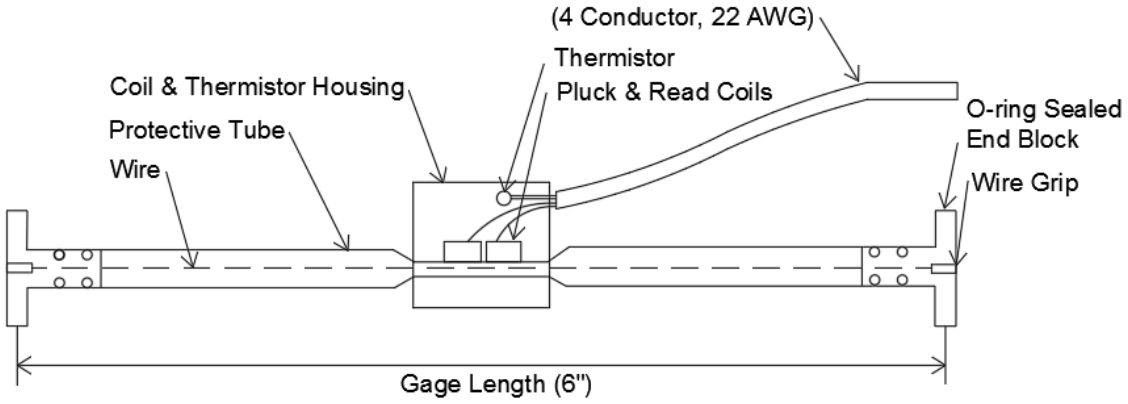

Figure 3.1: Vibrating Wire Gage

The enlarged ends of the VWG cause the gage to have the same strain as the encasing material. The tensioned steel wire, housed in a protective stainless steel sleeve, matches any displacement encountered in the concrete. VWGs are a relatively resilient gage and because the strains are a function of the mechanical properties of the tensioned wire, the gages can provide a stable measuring device for several years.

To complete the gage, the plucker and thermistor housing, coated in a molded epoxy, must be secured to the sleeve of the main body. The secure connection between the two allows the electronic plucker, consisting of two separate coils, to excite/vibrate the tensioned wire. For a completed interaction, the first coil, an electromagnet, is stimulated by an electronic signal. This signal induces a magnetic pulse to excite the tensioned wire causing the wire to vibrate. The second coil measures the natural frequency of the wire and returns the raw measured data to the data logging system. A frequency change in the wire indicates a length change that correlates to a strain in the concrete.

The thermistor lies next to the plucker wires. The thermistor measures the relative temperature at the gage. Temperatures may change rapidly due to the high temperatures of concrete curing, sun exposure, or sudden change in weather. The thermistor measures these changes to account for thermal effects affecting the concrete.

The plucker and thermistor are secured to the wire housing using hose clamps to prevent any slippage or gaps between the sensor and vibrating wire. At rest, the wire will have an initial strain of 2400 $\pm$ 200 micro-strains. Changes to the initial strain can be adjusted, using the tension collar, if the monitored area is expected to have large tension or compression. Initial strains can be checked prior to casting using a handheld device. The VWG's were designed to be embedded, in fresh concrete for strain measurements. These resolution of the gages are can be as accurate as $\pm 0.1\ \mu\varepsilon$, and designed to be

durable for monitoring construction projects including foundations, bridges, and containment vessels. Depending on the data acquisition system that is used, the reading of several gages can take several minutes since some systems evaluate each gage individually. This was the case of the monitoring system that was used in this study. The data logger is discussed in the next subsection.

3.4 DATA ACQUISITION SYSTEM

The data derived from the gages must be able to be transmitted from the sensors to a storage hard drive for analysis and comparisons. To complete the transmission, the gage must be connected to a processing and communication system where the raw data can be converted into usable information. The data logging system used in this project was a Campbell Scientific CR 3000 which was configured similar to the system used in a prior research study by Blok (2012). From the gages, the data travels through a series of devices until usable data is accessible and stored for the researcher. Figure 3.2 demonstrates the sequence of devices used for this setup.

Figure 3.2: Data Logging Sequence

The process of transmitting the data from the gages to the database begins with expanding the capacity of the number of usable gages. A single gage's lead wire connects directly into an AM16/32B Multiplexer, shown in Figure 3.3, which can record up to 16 VWGs. The Multiplexer operates one channel at a time until all of the connected channels (up to 16) are finished. The Multiplexer operates by stepping through multiple digital signals, and transferring the signals into a single source. Since these gages are

operated one at a time and require a fraction of a second to finish the reading, it may take a few minutes to read, if there is a large number of gages.

Once the Multiplexer completes its cycle, the data is input to the raw data processing unit. The AVW200 Analyzer, shown in Figure 3.4, is a processor that interprets the frequency readings collected from the Vibrating Wire Gage and converts it into different tables of strains and temperature. The Analyzer has two input ports that gages can connect directly into. However, the Multiplexer was used to increase the capacity of usable gages. If needed, two Multiplexers can be used for a maximum of 32 gages.

The information is then transmitted to the core of the logging system. The Campbell Scientific CR-3000 Data Logger, shown in Figure 3.5, is the central control of the whole system that runs the user's custom program, initiates the readings, records the data, powers the connected modules, and relays information to the communication devices. If wireless communication was not necessary, data can be downloaded directly from the logger. Operating the Data Logger is the Campbell Scientific PC400 interface software. This software creates a user defined program to direct the logger as necessary.

For the system used in this study, wireless communication from the logger was set up to enable access to the data from any location. The Raven XT phone modem and antenna, shown in Figure 3.6 and Figure 3.7, allow data to be collected from anywhere with Internet connection. The collection of data is generally the largest drain on the battery, but is necessary to collect every few days. If the data logger loses power at any point, all non-collected data is lost. The data collected shows the raw strain and temperature measurements from the gages as well as the voltage level for the power supply.

The logging system must have a secure power supply while being in a remote location. To minimize trips to the site, two Platinum Duracell AGM 12V 68Ah automotive batteries, shown in Figure 3.8, were chosen to power the system. The batteries used in the instrumentation could last approximately six weeks when data was recorded approximately once per hour. For a higher frequency, the battery life is less. The batteries were connected in parallel to increase their power capacity. Increasing the power capacity maximized the lifespan and minimized extra trips to exchange the batteries. The batteries were connected to the Data Logger through a charge regulator to avoid a power surge that would damage the system.

Solar panels were considered as an option to increase the lifespan of the batteries. Since solar panels need exposure to the sun, it would have been necessary to install mounting brackets to the end of the bent for the panel to have adequate exposure. Issues with solar panel include the possibility of the brackets interfering with the contractor, limited access to adequate sun exposure, and drilling into the bent cap. These options were compared to the ease of access to exchange the batteries. Access to the contractor's man-lift, close proximity to Ferguson Structural Engineering Lab, and expected lifespan of the batteries deemed the panels unnecessary for the bridges. As a result, the team decided to replace batteries at specific intervals to avoid recharging using solar panels.

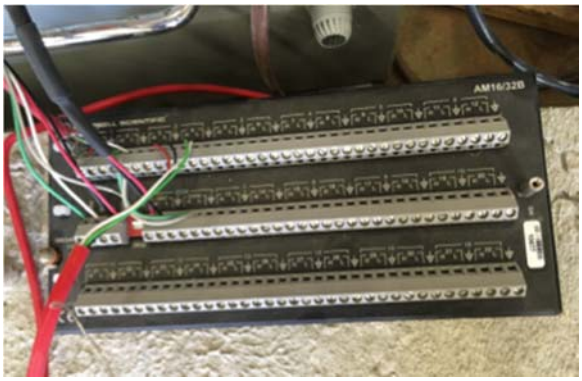

Figure 3.3: Multiplexer

Figure 3.4: AVW200 Analyzer

Figure 3.5: CR3000 Data Logger

Figure 3.6: Raven XT Modem

Figure 3.7: Antenna

Figure 3.8: AGM Battery

3.5 INSTRUMENTATION LOCATION

There are a number of considerations in developing an instrumentation configuration for a particular application. The sensor wiring needs to be protected from damage during concrete placement and in the completed structure. It is often desirable to minimize the length of the sensor wiring to reduce the likelihood of damage. On the other hand, the data logger and power source need to be put in a position that will minimize damage to these key components, while also locating these devices for easy access for any necessary maintenance or other situations that necessitate access. In addition, the location of the instrumentation needs to be selected to ensure safety of the research and construction personnel as well as the travelling public. In the case of this particular project, the safest location for the equipment was at a location that was not readily accessible to anyone passing by not associated with the bridge or project.

Since the equipment is electronic, it had to be covered and protected from any water and debris damage. Plastic storage containers, shown in Figure 3.9, were used to house the equipment. Separate storage boxes were used for the batteries and the data logging equipment. All devices used for the data logger were secured to a removable bottom in the container using small bolts. This limited the equipment from moving around and getting damaged as well as helping with organization. The wires from the VWGs were routed through a hole in the container, and then sealed using latex caulk. Desiccant bags were placed around the Data Logger to absorb any moisture that entered the housing unit.

Figure 3 9: Protective Housing Box

The batteries were placed in a separate container, but they were not secured since they needed to be exchanged periodically. Water damage was not as much of a concern for the batteries, so the container was primarily intended to protect from any debris during the concrete casting.

The data acquisition equipment was placed on the bent between girders to remain as close to the gages as possible and away from the travelling public. The equipment was accessible using a boom lift, which the contractors allowed the researchers to use.

3.6 GAGE LOCATION

The primary purpose of the project is to analyze the effectiveness of reinforcement in the negative moment region. To capture this behavior the gages were positioned at the critical location with the maximum negative moment, and therefore the VWG's were placed over the centerline of the bent where the two girders met. Typically there is approximately a 6 inch gap between the girders that the gages were centered over. The VWG was secured to the reinforcement bars of the concrete prior to casting using 1/2 inch plastic cubes and zip ties. The plastic cubes have semicircle grooves drilled out

to conform to the gage and reinforcement. The instrumentation layout and bridge geometries are described in detail in the following sections.

Once all of the instrumentation is placed and functioning properly, the equipment will be ready for the concrete to be poured. The data logger conducts strain readings multiple times per hour after the concrete is poured. The frequency of readings was a few times per hour during the early stages of the concrete. High temperatures during curing of the concrete are closely monitored. The frequency of data readings were reduced after shrinkage effects normalized and the strain levels are consistent.

3.7 OVERVIEW OF INSTRUMENTED BRIDGES

This section of the report introduces three newly-constructed bridges for the purpose of understanding the behavior in the negative moment region of bridges with partial depth PCP bridge decks. The geometries, instrumentation, construction process, and material properties of the three different bridges are discussed here. The first two bridges have been constructed and analyzed, while the third is still under construction with the expected completion date to be late 2017 or early 2018. The original goal of the field studies was to find continuous prestressed concrete girder applications utilizing partial depth prestressed concrete girders; however the research team was unable to find any bridges in Texas. . The first continuous span prestressed girder bridge with the PCPs had a construction schedule beginning in the summer of 2017.

In an effort to collect data for similar bridges, the project scope was redirected to bridges with simply supported girders with a continuous bridge deck (poor boy continuous) also utilizing PCP formwork. This change in bridge type reflects valuable information for the material behavior of the deck as it relates to shrinkage effects. Given the change in bridge focus, TxDOT provided detailed drawings of bridges that were to be

constructed within the desired time frame and having a relatively close proximity to Austin.

Meetings with the contractors and TxDOT personnel of the proposed bridges were conducted months before instrumentation. A clear plan was shared with everyone involved helped to clarify the research being provided for TxDOT, the interaction and time required between the contractors and researchers, and the time frame required of the project. This benefitted all parties to clear any confusion about expectations and how each party could benefit the other.

3.8 PROCEDURE OVERVIEW

The primary objective of the instrumentation was to capture the behavior of a bridge at a specific location. To begin the instrumentation, a process needed to be defined to determine the necessary steps for completion. This creates consistency between bridges and minimizes errors. Bridge geometries differ and present their own unique problems and solutions. A common procedure for instrumentation and construction is described below. Specific descriptions and procedures pertaining to each bridge are detailed in the subsequent sections.

3.8.1. Instrumentation

The instrumentation is intended to give an indication of the benefits of variations in the deck reinforcing steel in a given section of concrete. A reduction in the concrete strain and crack width was expected to correlate with the amount of steel. To get a comparison of the change in steel, three composite girder sections in each bridge were monitored. The standard TxDOT reinforcing consists of #4 bars spaced 9 inches on center each direction and serves as a baseline minimum amount of reinforcing for

comparisons. The other two sections had larger amounts of steel that were achieved by bundling additional reinforcement, either a #4 or #6, to the existing reinforcing.

Each monitored section had four gages strategically placed across the centerline of the bent. Three gages were attached to the top mat reinforcing, and were placed at the midpoint between girders over the PCP, at the edge of the PCP, and the center line of the girder as shown in Figure 3.10. The fourth gage was located directly below the third gage at the centerline of the girder to capture the strain gradient through the deck.

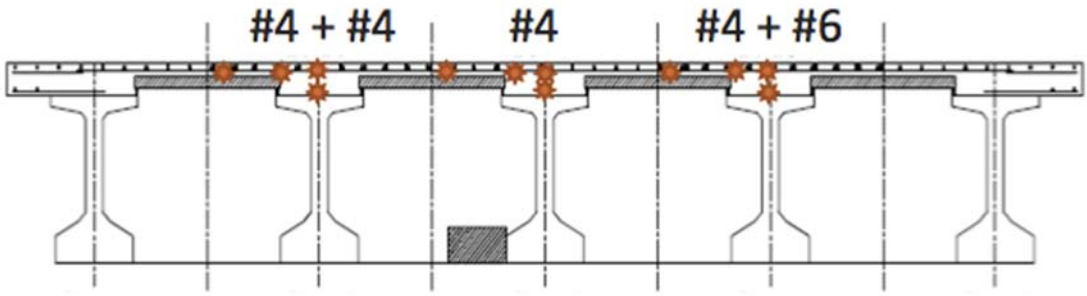

Figure 3.10: Overall Gage Layout

The first step for instrumentation was to examine drawings of the bridges, provided by TxDOT, to determine the ideal interior bent to monitor. Determining the gage location considered factors including the bridge cross-section, span length, safety, and accessibility. Drawings, provided by TxDOT, are described for each bridge in the following sections.

Once the gage locations were decided, a wire layout through the deck to the data logger was configured. The gages were ordered using the longest length of wire needed, and additional length of 10 ft. was added to each wire to ensure its ability to reach the data logger.

Becoming familiar with the bridge through the drawings as well as visits to the site was important for understanding how a bridge is constructed. Visiting the site before

the instrumentation helped to address issues not foreseen in the drawings. The installation could not begin until the contractor had finished placing the reinforcement for the bridge. Once the contractor had placed the reinforcement, about 7 days were available until the casting of the deck. Due to this constraint, site visits were conducted within the first 2 days after completing the reinforcement. This allowed adequate time to return to install gages and check for any issues before casting.

After assessing the site for any irregularities, the additional reinforcement was bundled to the existing reinforcement using twisting wire ties. The additional reinforcement length, for each side of the crack, was determined using the development length of a #6 in a concrete slab. Sample calculations for development length are shown in Appendix A. Once in place, the VWG was secured to the bar using plastic spacers and zip-ties. This system is quick and secure while ensuring the alignment of the gage remains parallel to the longitudinal reinforcement.

Once the VWGs were secured, the plucker and thermistor, with the lead wire, were attached and secured using a hose clamp around the gage. While securing the gage, precautions were taken to ensure the safety of the gage and wire.

The wire is the most vulnerable portion of the gage and must be protected. Any cut or break in the wires could render the gage useless and unable to provide reliable strain data. Figure 3.11 demonstrates the securing of the wires and gages. To protect the wires extending from the gage, the plucker housing was oriented for the wires to be on the underside of the reinforcement so as to minimize the likelihood of damage to the wiring from the vibrators used to consolidate the concrete during placement. As the wires extended from the gage toward the data logger, loops were made and loosely secured near the underside of the gage. After the loop, the wires were secured to the bottom of the reinforcement using zip-ties until they were able to exit through the bottom of the deck.

Collectively, these minimized the opportunity for anyone to snag the wires. If the wires did get caught, the loops provided strain relief by providing slack to minimize damage to the gage or it moving from its intended position.

Figure 3.11: Gages Secured to Reinforcement

In areas with the PCP, the foam-bedding strip was ideal for creating a hole to route the sensor wiring to the underside of the bridge. Silicone caulk was used to secure the wires from movement, and closed the hole created through the deck to minimize seepage of the fresh concrete during the cast.

The wires were routed through the hole until all excess wire was through the deck. To get to the Data Logger, the wires were routed along the top of the bent and between the girders until reaching the data logger housing.

The data logging equipment was assembled away from the construction site to save time and keep the equipment organized and safe. The housing box was placed at the

center of the bent to avoid obstructing construction and falling off the edge. The battery housing was placed next to the data logger housing. Once the housing boxes were in place, the gage wires were routed through on opening in the box and connected to the appropriate channels. Tags were placed on the gage wires prior to installment to ensure each gage location matched the recording channel. Tags were marked at the beginning of the wire near the gage and at the end where it plugged into the multiplexer. Once all of the gages were attached to the Multiplexer, the wires were coiled and placed as neatly as possible in the housing box as shown in Figures 3.12 and 3.13.

Figure 3.12: Wires in the Housing Box

Figure 3.13: Housing Boxes between Girders

An antenna that was connected to the modem was placed outside of the housing box to have access to open air and allowed remote communication with the data logger.

The batteries were connected to each other, then to the Data Logger to provide power for the system. After all of the wires from the gages and batteries were inside the data logging box, the hole the wires came through was sealed with the silicone caulk to minimize any water or debris entering the box.

To check the connection of the gages and make sure the Data Logger was running properly, a Verizon Hot Spot mobile Internet station was utilized. The mobile Internet

connection allowed access to the data logger via computer to check if all of the gages were properly reporting strain values. This check before casting gave a starting point for strain values that can be referenced for increase in strain. The check also will determine if there are any damages that occur during the installation.

3.8.2. Construction Practice

The contractor made use of several pieces of equipment to obtain a good finish on the concrete deck. Figure 3.14 shows the concrete finishing machine (screed) that maintains the proper deck thickness and good finish to the deck. The screed travels along the bridge on rails placed at the two edges of the bridge. The rails are checked using a GPS surveying range finder. This ensures the screed creates a uniform top-of-slab elevation at any point along the rails. The screed rails are attached to brackets on the side of the bridge as to not interfere with any of the cast concrete.

Figure 3.14: Bridge Screed

The casting of the concrete took place in the middle of the night to minimize interruption in traffic to the street below the bridge as well as avoid the heat of day that can lead to rapid loss in water due to evaporation. The gages were inspected a few hours before the cast for their correct position, secured tight, and their wires properly covered. Many gages become loose as the reinforcement shifted during the week leading up to the cast. Additional zip-ties were added to any loose gages. .

The casting procedures were monitored closely for any accidents that could have altered the readings of the gages. Any noticeable irregularity was observed and recorded to be replicated as closely as possible in future analysis.

Before casting the concrete, the deck was sprayed with water to hydrate the pre-cast elements, such as the girders and panels, and eliminates them absorbing water from

the cast concrete. If the pre-cast elements absorb too much water from the cast concrete, delamination could occur between the two layers.

The concrete was delivered to the deck via pump-truck shown in Figures 3.15 and 3.16. Pump trucks can deliver concrete at a rate of approximately 180 yd^3/hr. This volume of concrete is fast moving and continuous as long as concrete trucks are available. The high impact from concrete at that rate can lead to damage to the gages if proper care is not taken.

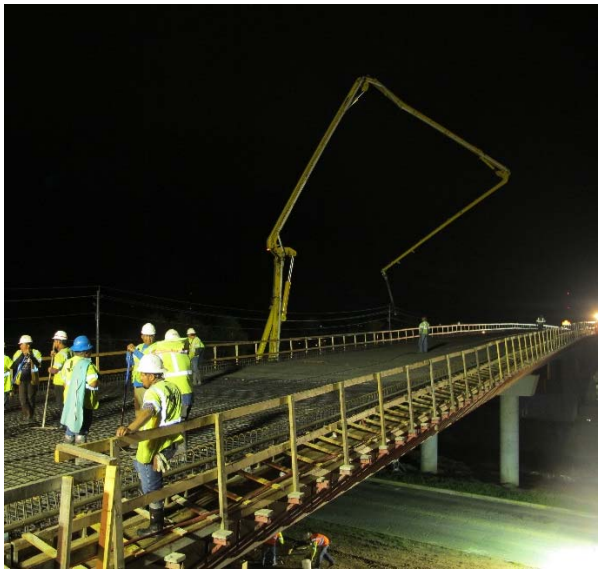

Figure 3.15: Concrete Pump Truck

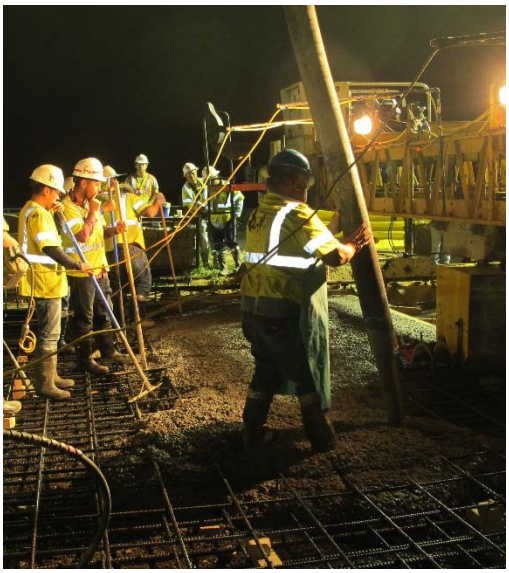

Figure 3.16: Casting Crew

As the concrete is poured, concrete vibrators consolidate the mixture to the bottom of the deck. As the bridge screed moves along the length of the girders, a finish carriage alternates back and forth in the transverse direction. The finish carriage, shown in Figure 3.17, is made up of rotating augers to consolidate the top surface of concrete and a drag plate to flatten the surface. Any low spots in the concrete that were not

affected by the finish carriage were filled in with concrete by a shovel. The bridge would move back then pass over again with the finish carriage.

Figure 3.17: Finish Carriage

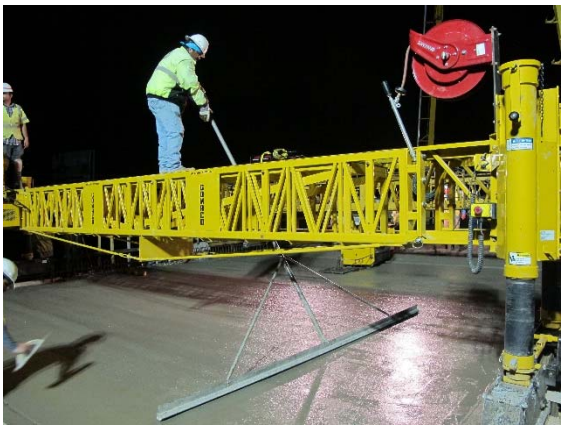

Figure 3.18: Finishing the Surface

An additional finishing bridge on the rails closely followed the screed. The finishing bridge served as a walking platform for the surface finishers shown in Figure 3.18. The surface finishers used a large broom to remove any excess pooled water as well as create a roughened surface.

A third mechanical bridge utilized a chemical compound sprayed on the deck to seal the curing surface. The chemical seals the top surface and prevents seepage into the concrete. This seal can greatly increase the lifespan of a bridge.

To finish the concrete surface, the contractor placed a wet burlap coving on the concrete as shown in Figure 3.19. This wet surface helps to retain the moisture. The reduction in rate of moisture loss helps to reduce cracking and prevents a strain gradient forming through the deck. The burlap is typically left on for one to two weeks.

Figure 3.19: Burlap Covering

Concrete test cylinders were taken so as to provide material testing samples of the concrete over the gages. A concrete mix design of 4 ksi is specified for the bridge deck, but to represent the exact concrete in the area of monitoring, the concrete at the gages was recorded and tested as shown in Figures 3.20 and 3.21. A concrete slump test as well as 4 in. concrete cylinders were made following the ASTM C39 and C143 standards.

Figure 3.20: Cylinder Testing

Figure 3.21: Slump Test

Once the casting of the deck was complete, the gages were permanently sealed in the concrete. The gages were checked to make sure their strain readings were similar to their initial readings. If strain readings were unusually high or low, this could indicate the gage or the wire had been damaged. If the strain readings were similar to the initial reading, the gage was tared and set to zero.

3.8.3. Monitoring

Monitoring of the bridge consisted of continually recording the strains from the gages as well as observing the construction sequence happening at the bridge. Monitoring the construction activity helps to create correlation between any changes in the measured strain. Events on the bridge can include removal of the moisture barrier, large vehicles on the bridge, quick changes in weather, and additional construction.

After the completion of the deck, the bridge was monitored until the shrinkage strain had normalized and live load testing was complete. Since shrinkage strain continues over the lifespan of the material, the bridge was considered to have reached a normalized shrinkage strain level near 80-90% of the maximum shrinkage. This typically occurred within the first month of monitoring.

The second milestone for monitoring was the live load testing. This was dependent on the schedule of the contractor and when the bridge was opening to traffic. The live load test included two tandem-axle trucks each filled with sand to be placed on the bridge deck. The trucks represent a known load on the bridge that correlates to a measured strain from the gages. Each truck axle was weighed then placed at specific locations marked on the bridge. Locations for the different configurations were marked using field marking spray paint. To define the location of the truck, the bridge was marked for the location of the driver side front tire to be centered on. From the marked

locations, five truck configurations were used to maximize both the negative moment at the gage location and the mid-span deflections of each span. The mark was made using lines to center the tire from the side and the front as shown in Figure 3. 22.

Figure 3.22: Tire Location Mark

For the first three test configurations, the trucks maximized the negative moment at the gages. A single truck was centered at the mid-span of the same beam line of each span shown in Figure 3.23. An X marks the center of each of their masses. This was intended to maximize the moment over a single beam line. After readings were taken for the test, the trucks were moved to be centered on the next instrumented beam line.

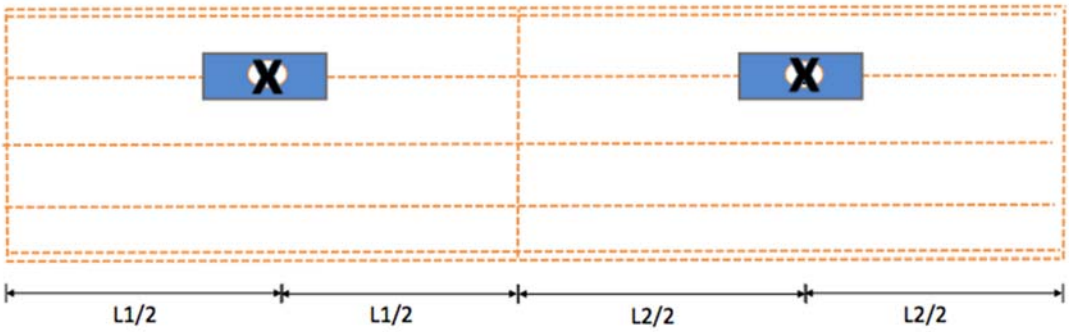

Figure 3.23: Single Girder Live Load Test

The last two tests maximized the deflections in one span at a time. These tests centered the trucks side-by-side at the mid-span of a single span. The X shows their combined center of mass. Their combined weight was centered at the centerline of the deck shown in Figure 3.24.

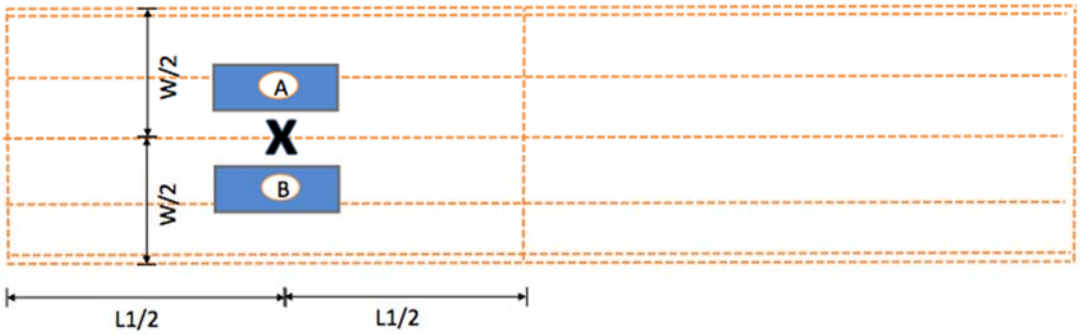

Figure 3.24: Single Span Live Load Test

Since it took a few seconds to register a reading from each gage, the truck positions were maintained in the same position for a minimum of 2 minutes to get five readings. While in position, any cracks in the deck over the bent were traced and recorded, and deflection readings were taken below the bridge using a laser range finder. The laser range finder provides a measure of the distance from a static benchmark point. Therefore, initial readings with no trucks or other superimposed loads were first recorded. For each desired location, 3 readings were taken and averaged to establish the initial

position of the girders. The process was then repeated with the trucks in position to establish the position of the girders with the load. The deflection was then found by subtracting the initial readings from the second readings. After strain and deflection readings were taken, the trucks were completely removed from each span before being guided to the next location. This negated temperature effects to provide an initial strain reading for each test.

Once all tests were completed, the monitoring instrumentation was disassembled and removed from the site. For future testing and monitoring of the bridge, the wires remained accessible. The gages remain embedded in the concrete and their wires below the deck were neatly coiled and secured to the top of the bent. The data logging equipment and batteries were removed for the next bridge instrumentation.

3.9 SAN MARCOS SH123 BRIDGE

The first bridge available for instrumentation was located in San Marcos, TX. The bridge was part of a highway expansion involving an overpass and frontage road expansion. The overpass consisted of North and South entrance ramps developing into a three span bridge. Two North/South lanes and a shoulder service each direction. Each half of the bridge is made of two completely separate structures. The bridges share entrance ramps and abutments, but have independent foundations and superstructure with a one inch gap between the decks. Instrumentation was utilized only on one bent of the East half of the bridge.

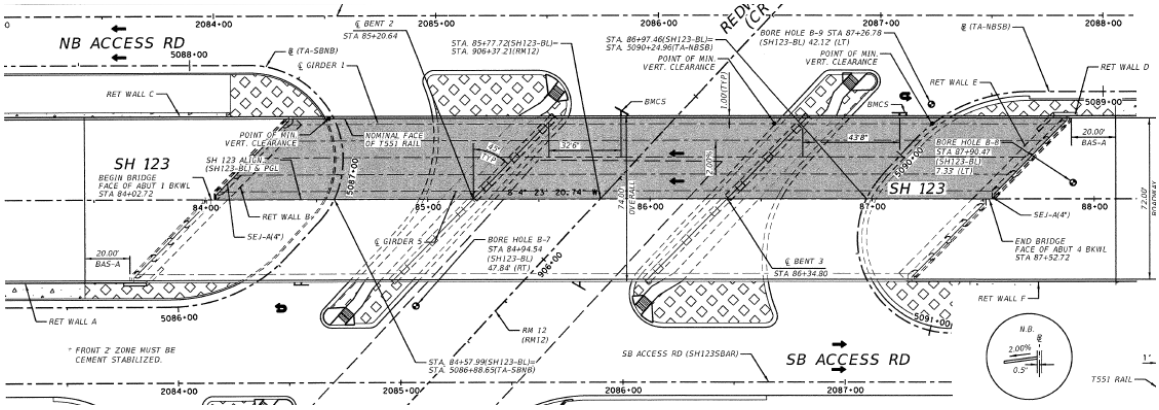

Figure 3.25: SH123 Plan View Drawing (TxDOT)

A partial set of plans as shown in Figure 3.25 and 3.26, were provided to examine the layout of the bridge. From the sheets, 5 girder lines were being used for each of the two halves of the bridge. This allowed the application of gages to be applied to three interior girders. By using only interior girders, direct comparison between the girders can be achieved as they have similar support conditions. The deck utilized #4 @ 9 in each direction with longitudinal bars on top for the top mat reinforcing.

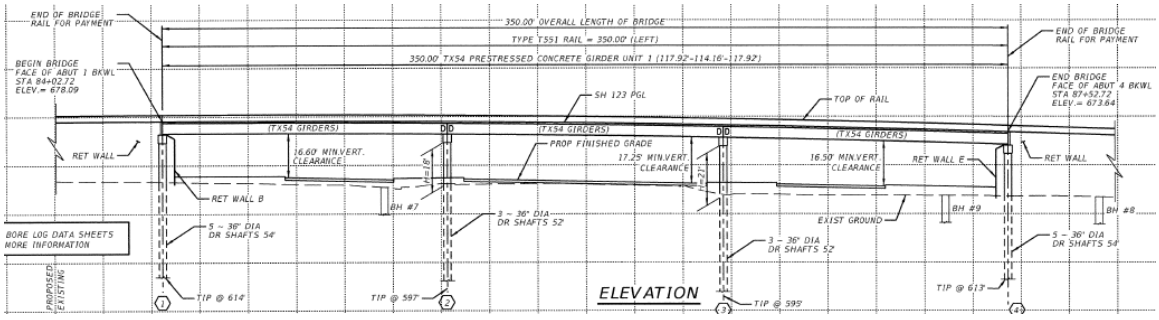

Figure 3.26: SH123 Elevation View (TxDOT)

The area of instrumentation was to be located over the interior bent. Access to the underside of the bridge would be necessary to be able to change batteries and access the data logger. Since the bridge had identical first and third spans, either interior bent should provide similar data. Below the bridge, Redwood Road, remained operational during the

construction of the bridge, which therefore limited some access to the underside. Part of the intersection was under construction as U-turn lanes were being installed on both sides for the frontage road. This construction allowed access to the bottom of the bridge without the concern of traffic interference. The Northern interior bent was selected to be instrumented after considering ease of access.

Before the instrumentation installation, a site visit helped to evaluate what the options were for the gages. After getting to the site, it was apparent that the PCP's were not continuous over the bent. Due to the harsh skew of the bridge, Permanent Metal Deck Forms (PMDF) as shown in Figure 3.27 and 3.28, were used over the bents in accordance with standard TxDOT details. This altered the section over the bent as the deck acted as a full depth cast-in-place deck. This did not align to the original intent of the project, but still provided beneficial data for comparisons of bridge behavior.

Figure 3.27: Permanent Metal Deck Form

Figure 3.28: Reinforcement over the PMDF

Three interior girders were selected to be instrumented with varying reinforcement details. Gages 1-4 monitored the first section containing one additional #4 bar bundled to the existing longitudinal steel. Gages 5-8 monitored the second section containing the standard reinforcing. Gages 9-12 monitored the third section containing one additional #6 bar bundled to the existing longitudinal steel. Figure 3.29 shows the layout of the gages.

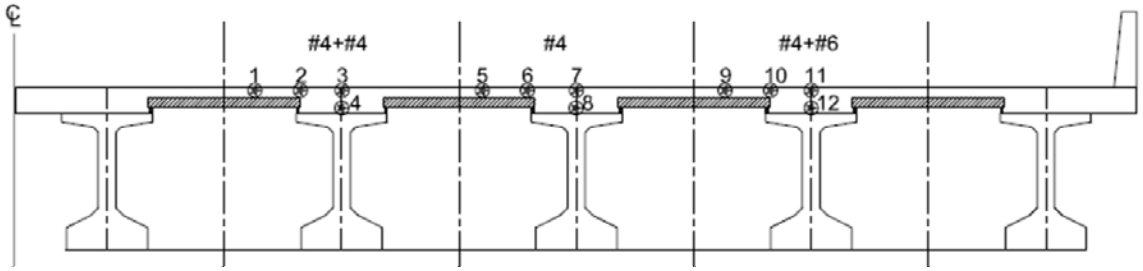

Figure 3.29: Gage Layout

Crack formers were used to be able to control the location of cracks. As the bridge was inspected, a two-inch steel angle was placed as a crack former from the bottom of the deck. This angle ran along the centerline of the bent and was directly between the ends of the girders. The location proved to be an issue and interfered with the intended gage locations. Since it was at the bottom of the deck and at the center of the bent, the bottom gage had opposition to where the gage was intended to be placed. To be able to capture a strain gradient through the depth of the deck, the gages were placed immediately next to the angle as shown in Figure 3.30, in an attempt to best represent the intended strains. Because of the shift in the bottom gage, the gage for the top of the deck was shifted to match the location.

Figure 3.30: Top and Bottom Gages

Figure 3.31: Gage at the Edge of Girder

As described in the previous sections, the additional steel was bundled to the existing reinforcement (#4 @ 9 in. each direction). Once bundled, the gages and wires were secured using zip ties as shown in Figure 3.31. When exiting the bottom of the deck, the wires needed to be protected from being cut by the sharp edges of the PMDF. A silicone sealant was used to secure the wires from movement and avoid being cut by the metal, shown in Figure 3.32.

Figure 3.32: Wires passing through the deck

The data logging equipment was setup and placed between the girders as described in the previous section.

The casting of the deck occurred on October 15th at 2 am with the use of a pump truck shown in Figure 3.33. Before any casting began, the gages were checked to ensure proper function, as well as secure any gages or wires that had become loose as shown in Figure 3.34. No obstructions or interferences with the gages was noticed during the cast.

Figure 3.33: Concrete Trucks

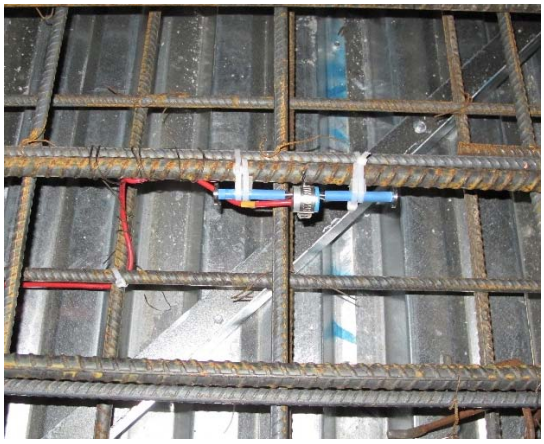

Figure 3.34: Securing Gages

As the concrete was poured over the instrumentation area, concrete for testing were collected. A slump test showed the concrete to have a slump of 7 inches which is within the allowable limit. After the concrete was approved, twelve 4-inch cylinders were collected.

Table 3.1: Concrete Mix Design

f'_c (psi)	w/c Ratio	Fly Ash	Hydraulic Cement	Coarse Aggregate	Fine Aggregate
4000	.45	67%	33%	58%	42%

Live load tests were conducted before the bridge opened to traffic. The test included five truck configurations discussed below using tandem-axle trucks filled with

sand provided by the local TxDOT Maintenance Facility. Once the trucks were loaded with sand, axle weights were taken at a highway DOT Inspection Station. Truck dimensions and axle weights are given in Figure 3.35.

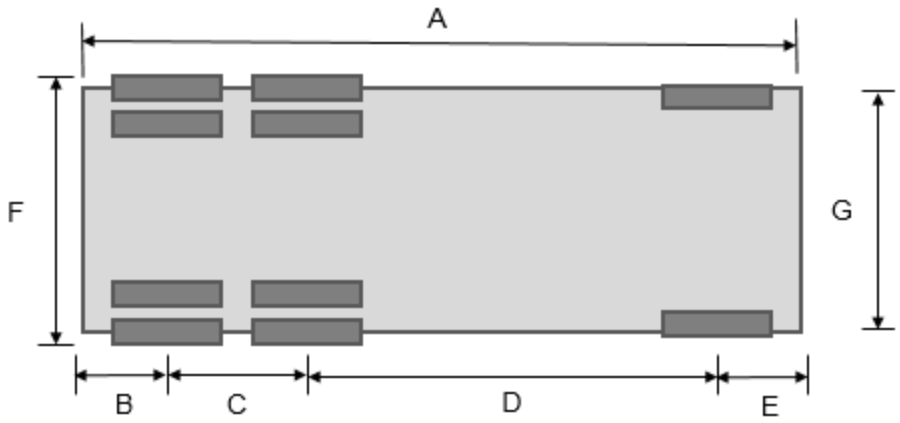

	A	B	C	D	E	F	G	Rear Axle	Front Axle	Total
Truck A	288”	36”	54”	169”	29”	96”	78”	36,780lb	12,660lb	49,440lb
Truck B	284”	34”	54”	167”	29”	97”	83”	37,440lb	11,660lb	49,100lb

Figure 3.35: Truck Dimensions and Axle *Weights*

Truck locations are shown in Figures 3.36 (a)-(e).

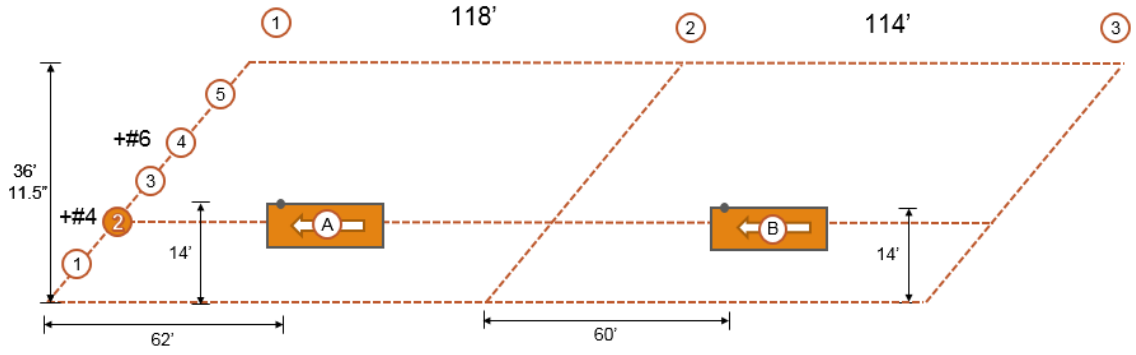

(a) Load Case 1

Figure 3.36 continued next page

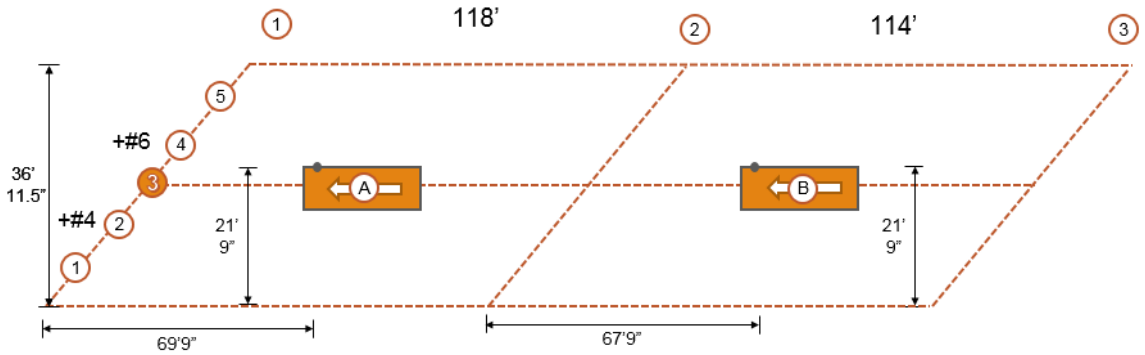

(b) Load Case 2

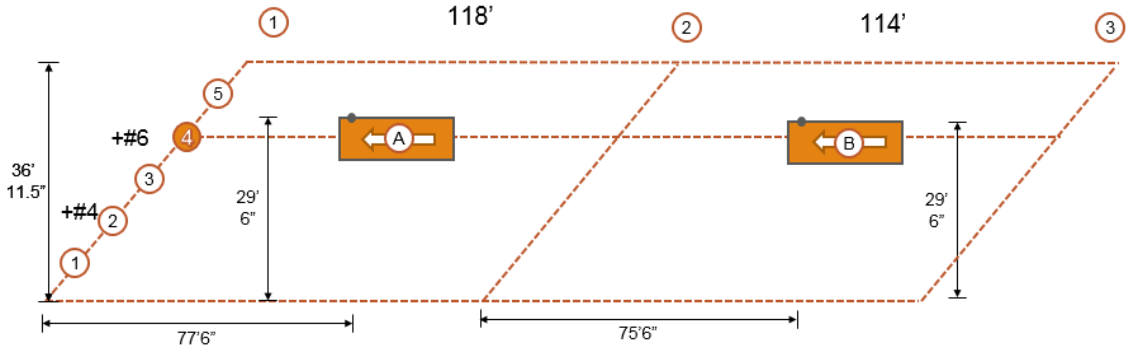

(c) Load Case 3

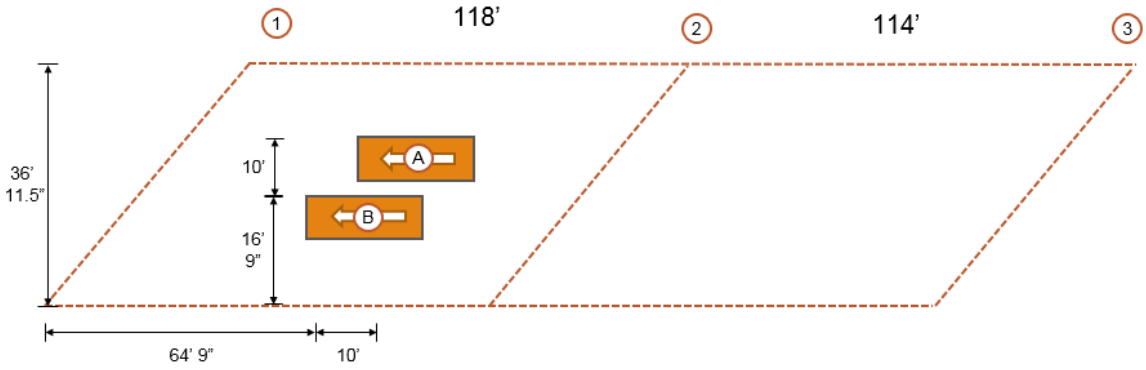

(d) Load Case 4

Figure 3.36 continued next page

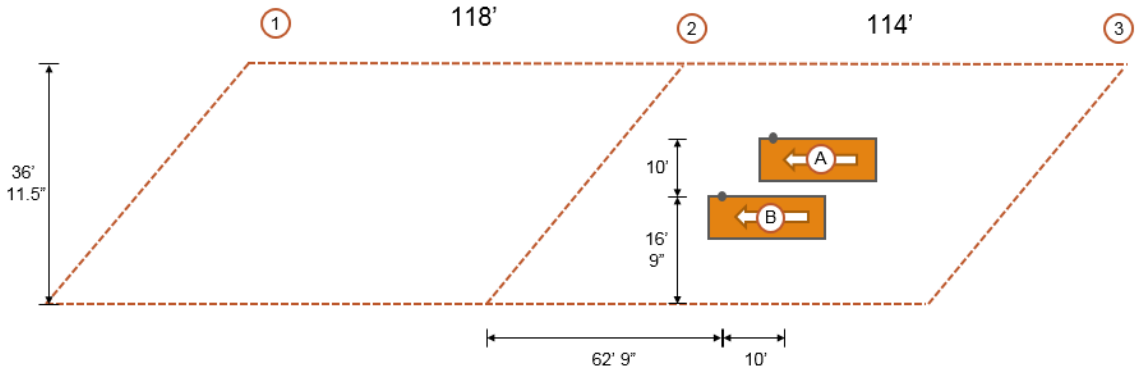

(e) Load Case 5

Figure 3.36 (a)-(e): Truck Configurations

The bridge was marked for the truck locations the day before testing to minimize the time of testing and to minimize errors. During the test, trucks were guided to the marked spots to ensure their position. Since the bridge was at a 45 degree skew, the mid-span of the girders were not side-by-side. The trucks matched the skew angle as shown in Figures 3.37.

Figure 3.37: Side-by-Side Trucks (offset by skew angle)

Monitoring of the bridge lasted for a total of 155 days until the bridge was opened to traffic. During this period of monitoring, construction was completed then opened to traffic. Any irregularities in the strain recordings will be mentioned in detail in the following chapter.

3.10 BASTROP SH71 ENTRANCE RAMP

The second bridge provided was located in Bastrop, TX. This bridge was an entrance ramp onto the highway from the frontage road as part of a reconstruction project to the area. The bridge consisted of four beam lines of simply supported girders with 5 spans. The top mat reinforcing is #4 @ 6 in transverse bars on top and #4 @ 9 in longitudinal bars on bottom. The bridge crossed over active railroad tracks, a river, and two operational street turn-arounds. Each of these needed to be considered to be able to access the instrumentation while remaining safe and minimize interference.

None of the five spans were identical as shown in Figure 3.38, so choosing the location of the gages needed to capture the largest negative moment produced in the bridge. Not only were span lengths inconsistent, girders changed size over the tracks, and expansion joints were placed every two spans over the bent. This eliminated half of the options for the bents to instrument.

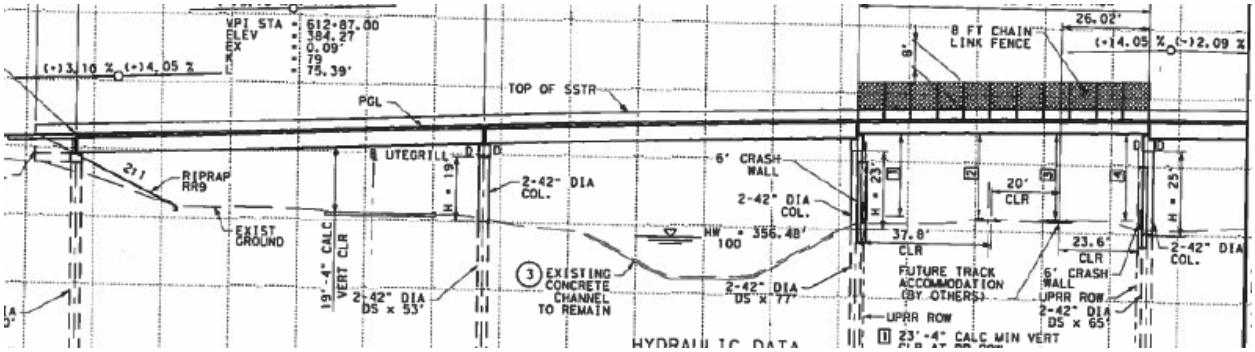

Figure 3.38: SH71 Elevation View Drawing (TxDOT)

The location of the gages had to be safe to access from below, have similar span lengths and girder sizes, and not be at an expansion joint. The selected interior bent between Span 1 and Span 2 as shown in Figure 3.39, consisted of similar span lengths and girder sizes, but had a CIP portion of the deck over an exterior girder. The CIP portion routed a drainage pipe along the deck and required a thicker full-depth slab. This issue was deemed to be inconsequential as the CIP portion was limited to only one of the exterior girders. The other three girders would still use the PCP system. However, this did eliminate the possibility of having a fourth girder to instrument.

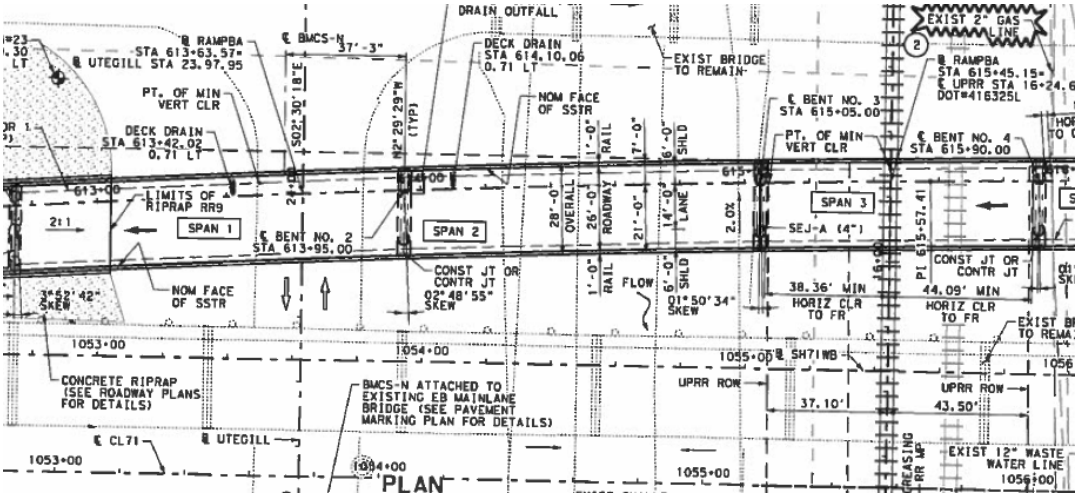

Figure 3.39: SH71 Plan View Drawing (TxDOT)

The top mat reinforcement was used over the length of the bridge, with the transverse steel on top. The reinforcement remained constant over the whole bridge other than over the bents where intermediate 5 ft. #4 bars had been added at 4.5" spacing between the standard bars as shown in Figure 3.40. These were placed in accordance to TxDOT's details for PCP over bents as shown in Figure 3.41, in anticipation of controlling cracks forming at that location.

Figure 3.40: Additional Reinforcement

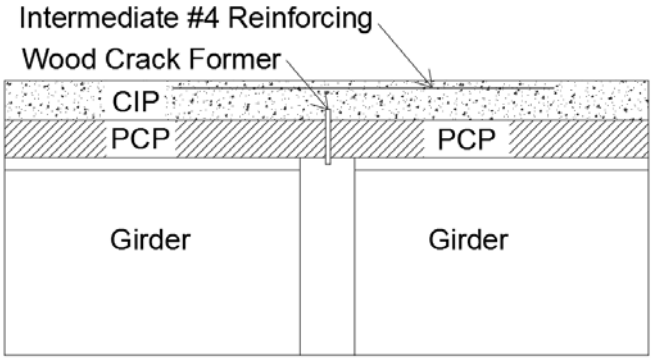

Figure 3.41: TxDOT Detail

Adding reinforcement to the existing steel would make the concrete too congested to be able to get the desired relationship between the area of steel and measured strain. To get the intended three areas of steel in the section, the steel had to be adjusted. Figure 3.42 shows the steel layouts with the gages. Starting from the South side, the intermediate steel was removed over the exterior girder to reduce the steel down to the standard reinforcing of #4 @ 9 in. The steel over the first interior girder was not adjusted and remained at #4 @ 4.5". The steel over the second interior girder had one additional #4 bar added to the primary longitudinal bars to mimic the same area of the bundled #6 used in the San Marcos Bridge.

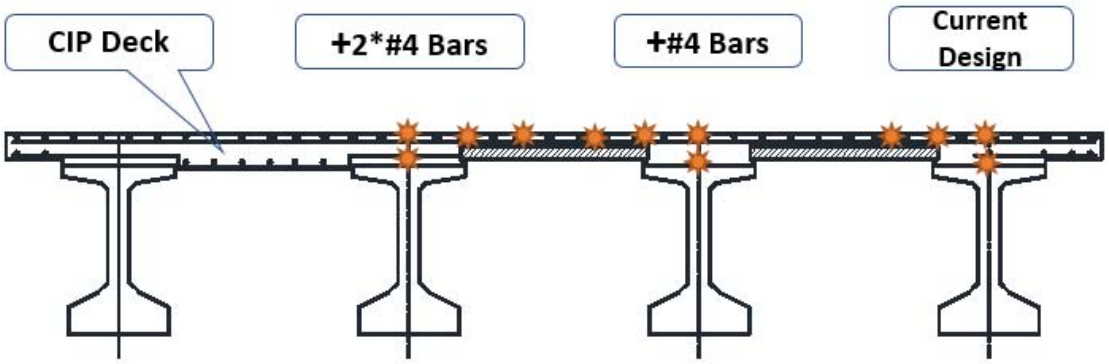

Figure 3.42: Gage Layout

The crack former in this bridge differed from the previous since the PCP were continuous across the length of the bridge. Over the center of the bent, a ¾ in. timber board was secured between two panels as shown in Figure 3.43. The wood extended from the top of the girders to one inch above the panels, and was continuous across the width of the deck. This strip created a weak joint in the deck for a crack to form. The gages were placed directly over the crack former to ensure the gage captured the strain across the crack.

Figure 3.43: Wood Crack Former

The top layer gages had no interference with the crack former as the longitudinal reinforcement remained above the strip, and were carefully placed directly over the crack former to ensure the gages captured the strain across the crack as shown in Figure 3.44. For the strain gradient, the bottom layer gages had to pass through the timber board as shown in Figure 3.45. With permission of the contractor, holes were drilled in the wood to allow enough clearance for the gage and the attached reinforcement bar to fit through the wood strip.

Figure 3.44: Top Layer Gages over the Crack Former

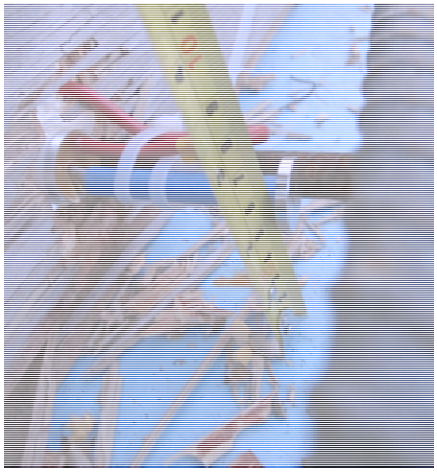

Figure 3.45: Gage through the Crack Former

The concrete cast occurred on March 13th at 2 am. Since the contractor for the bridges in Bastrop and San Marcos were the same, similar procedures, shown in Figure 3.46, were conducted for the casting of the deck. However, collecting material testing samples differed from San Marcos. In addition to the twelve 4-inch concrete cylinders, Modulus of Rupture beams were cast to get more samples for tension testing. The concrete had a slump of 4.5 in.

Figure 3.46: Screed Bridge

The mix design for the CIP layer is listed in Table 4.2 below.

Table 3.2: Concrete Mix Design

f'_c (psi)	w/c Ratio	Fly Ash	Hydraulic Cement	Coarse Aggregate	Fine Aggregate
4000	.45	67%	33%	58%	42%

Live load testing was conducted with the same five configurations. Two trucks were provided by the local TxDOT Maintenance Facility. Since there was no DOT Inspection Station nearby, the county Commercial Vehicle Enforcement (CVE) Patrol Officer assisted in getting axle weights. The officer used single tire scales to measure the axle load as shown in Figure 3.47. Dimensions and axle loads are given in Figure 3.48.

Figure 3.47: Single Tire Scales

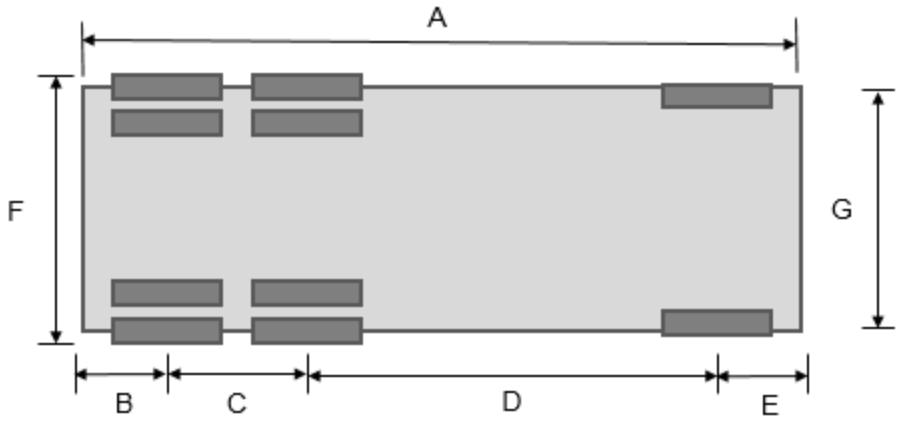

	A	B	C	D	E	F	G	Rear Axle	Front Axle	Total
Truck A	288”	36”	54”	169”	29”	96”	78”	36,780lb	12,660lb	49,440lb
Truck B	284”	34”	54”	167”	29”	97”	83”	37,440lb	11,660lb	49,100lb

Figure 3.48: Truck Dimensions and Axle *Weights*

The test truck configurations are shown below in Figure 3.49 (a)-(e).

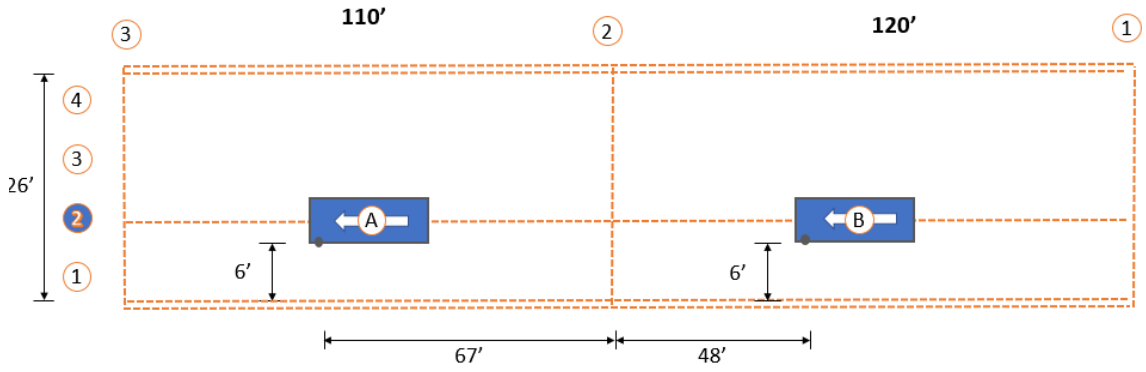

(a) Load Case 1

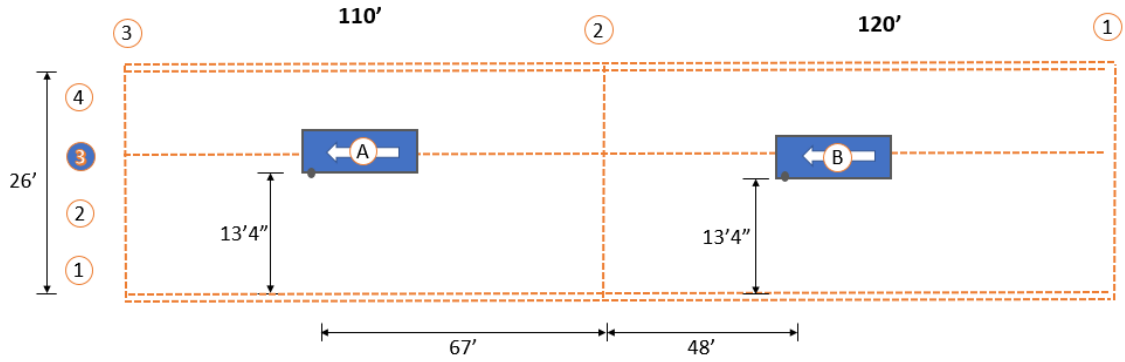

(b) Load Case 2

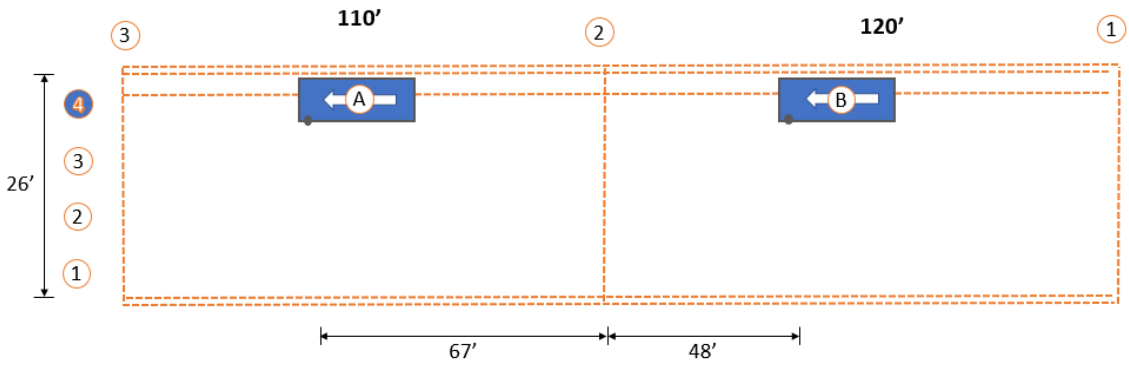

(c) Load Case 3

Figure 3.49 continued next page

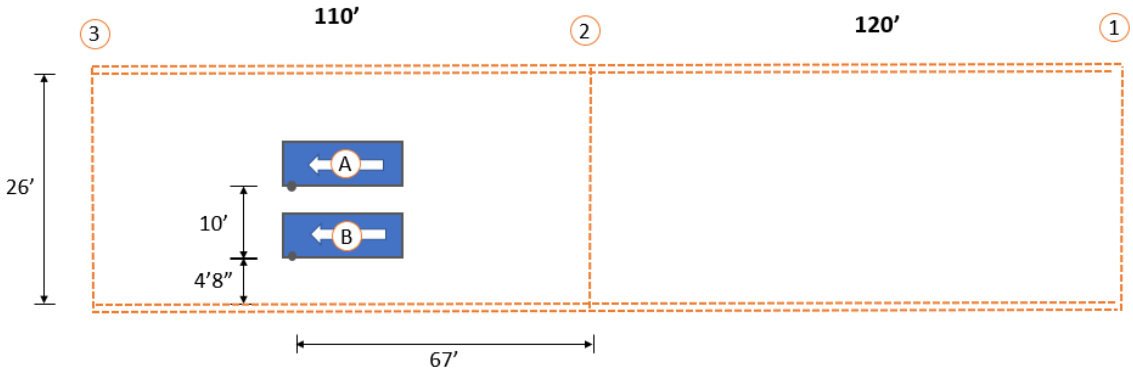

(d) Load Case 4

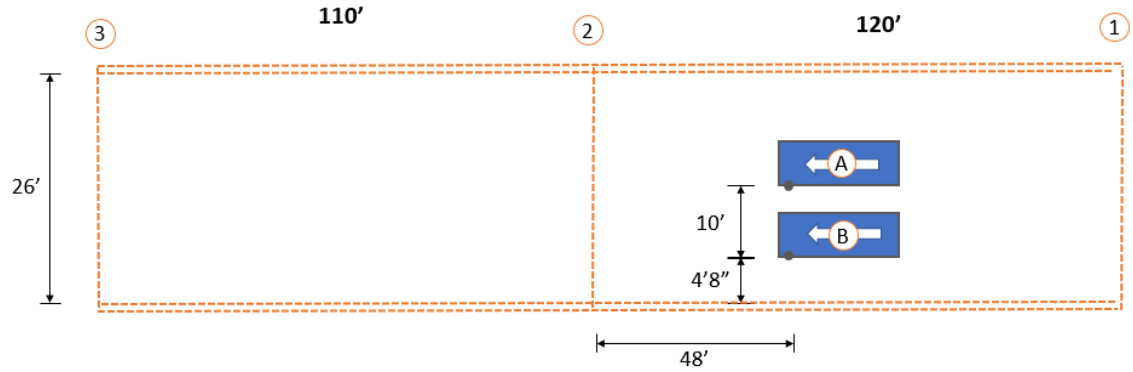

(a) Load Case 5

Figure 3.49: Truck Configurations

The deck was marked and the trucks were guided to their locations. After each reading, the trucks were moved completely off the span before moving to the next position as shown in Figure 3.50.

Figure 3.50: Removal of Truck from Span

Figure 3.51: Single Girder Configuration

Each instrumented girder required trucks to be centered over the girder centerline as shown in Figure 3.51. Since the exterior girder was at the edge, the trucks were moved as close to the guard rail as possible as shown in Figure 3.52. The strain from the exterior girder will be accounted for in relation to the location of the truck. The side-by-side position had to be carefully done as there was not much additional room as shown in Figure 3.53.

Figure 3.52: Exterior Girder Position

Figure 3.53: Side-by-Side Position

Shortly after the live load testing was completed, the bridge was opened to traffic. This concluded the testing period, and the instrumentation was removed from the bridge.

The gages and wires remain permanently with the bridge. Extra wire was secured to the top of the bent, and remains available for future monitoring of the bridge.

3.11 ROUND ROCK UPPR RAMP

The final bridge for monitoring for this portion of the project is located in Round Rock, TX. This bridge and its instrumentation will be outlined and detailed, but will not be constructed before the completion of this report. Although this bridge monitoring is not recorded yet, its importance should be noted as it is the sole bridge that aligns with the project's original intent.

The bridge consists of two, multiple-span ramps for IH 35 at the intersection of SH 45 in Austin, TX. Ramps 20 and 21 are the first continuous span bridges for this project, and the first of their kind in Central Texas. They each consist of three continuous spans of spliced pre-stressed concrete girders with post-tensioned connections with similar structural details. The bridges use four beam lines with the PCP formwork and 4.5 in. CIP for the deck, and a reinforcing layout of #6 @ 4.5 in. longitudinal bars on top with #5 @ 5.5 in. transverse bars on bottom over the continuous bents. The first and third spans are identical as shown in Figure 3.54, leading to either interior bent producing similar monitoring data. The continuous bridge portions span over an active rail road track and street open to traffic. Access beneath the bridge is uninterrupted, and will allow access to the data logging equipment when necessary.

Ramp 20 was selected as the bridge for instrumentation as it will be completed first. Since this bridge fits each criteria of the project objective, extensive instrumentation will be used. Due to the four beam lines as shown in Figure 3.55, limiting gages to only interior girders is not an option. Each of the girders will be instrumented to allow a direct

comparison between exterior and interior girders. Along with each girder, both interior bents may be instrumented.

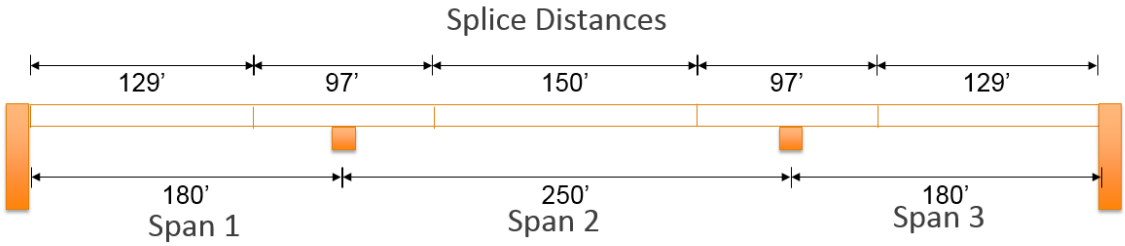

Figure 3.54: IH 35 UPPR Ramp Elevation View Drawing

A VWG layout will be used in the CIP layer similar to the previous bridges. In addition in the deck, gages will be mounted to the exterior of the girders over the bent. This will help to determine strain from the top to bottom, as well as give insight into the behavior of the bridge as a whole in the negative moment region.

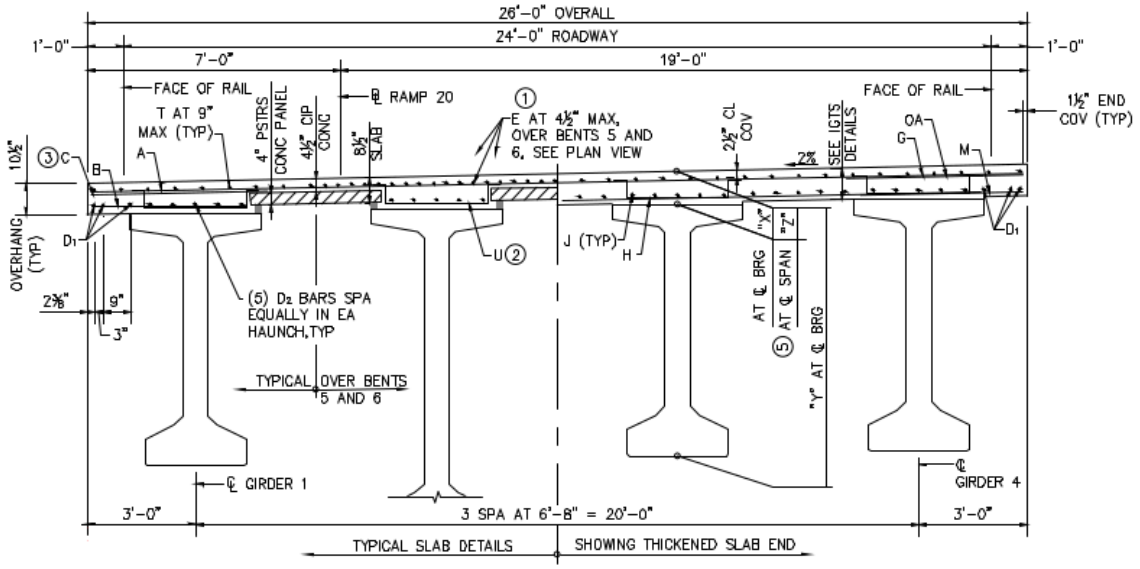

Figure 3.55: IH 35 UPPR Ramp Section View Drawing (TxDOT)

The concrete mix design is shown below in Table 3.3.

Table 3.3: Concrete Mix Design

f'c (psi)	W/C	Fly Ash	Hydraulic Cement	Coarse Aggregate	Fine Aggregate 1, 2
4000	.45	29%	71%	58%	30%, 13%

Chapter 4: Instrumentation Results

4.1 INTRODUCTION

This chapter provides a summary of the data gathered in the field monitoring studies at the bridges in San Marcos, TX and Bastrop, TX. In addition the strain data, comparisons and observations on the behavior of the two bridges are provided. Each bridge was monitored from the casting of the deck until open to traffic. As outlined in Chapter 3, the strain gages were placed in the deck at the location above an interior support and three different longitudinal reinforcement configurations were used for each bridge to determine the impact of the reinforcement on the deck cracking and corresponding strains. The data was treated in such a way to isolate the deck strain from the variety of sources that influence the gage readings. The chapter has been divided into five sections. Following this introductory section, and overview of the sources of the strains and the methods used to isolate the different components of the strains are provided. The next two sections focus on the data gathered from the two different instrumentation efforts. Finally, a summary of the chapter is provided in the last section.

4.2 ISOLATION OF STRAINS FROM DIFFERENT SOURCES

Figure 4.1 shows that the measured strains from the gages can have strain components from four sources: temperature, shrinkage, creep, and mechanical strains. Isolation of the strain components can be a difficult process; however steps were taken to identify the specific strain components. Changes in strain due to temperature fluctuations can be divided into two primary categories: 1) changes in the ambient temperature, and 2) thermal gradients as a result of solar exposure. In general, the bridge superstructure follows the classic behavior of thermal expansion. Increases in the temperature cause the

concrete material to expand, while decreases in the temperature cause the material to contract. The strain rate is generally dependent on the aggregate used in the concrete mix. In general, there are two volumetric changes that are of interest with the concrete, and they are referred to creep and shrinkage. Creep strains occur due to the connection between the CIP layer and precast elements that utilize pre-stressing. Shrinkage is the main contribution to deck strains, and cause concrete to shrink as the cement paste dries. Typically, the majority of the shrinkage occurs within the first few weeks after casting. A complexity of this shrinkage issues in these bridges are the significant difference in the age of the concrete between the precast concrete girder, the PCPs, and the cast-in-place (CIP) portion of the deck. Often the precast elements are months older than the CIP layer and have already experienced the majority of their shrinkage. The restraint of shrinkage from boundary conditions between the CIP and precast elements may induce cracking.

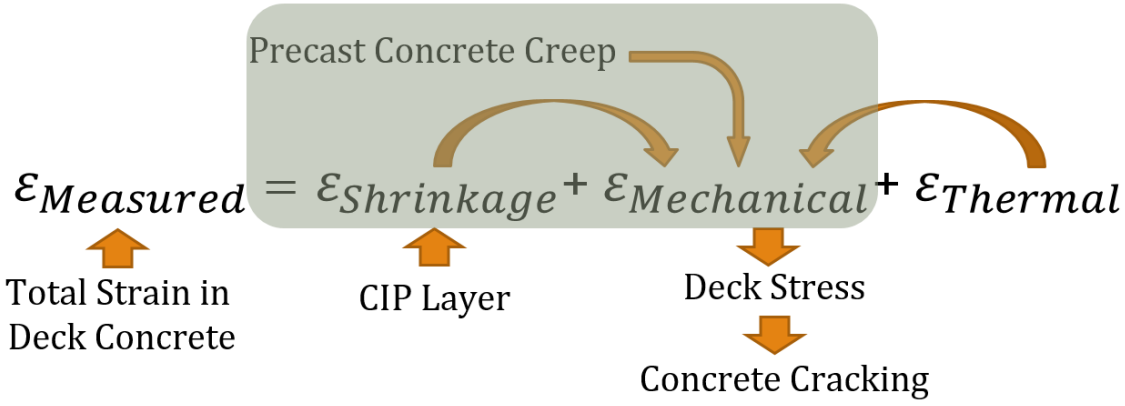

Figure 4.1: Strain Sources

4.2.1. Temperature Correction

Temperature strains can be isolated and accounted for using various methods. Since all of the gages include a thermistor for temperature readings, the temperature at

each gage location could be determined. The Geokon VWG manual described a method to compensate for temperature fluctuations. Temperature changes in the deck can cause issues, as changes in strain due to temperature can create a cracking strain as the concrete is restrained by other members. Changes in temperature can also change the tension in the vibrating wire which can cause the gage to indicate compression when the wire has lengthened causing slack. If the coefficients of concrete and steel were the same, equal and opposite expansions would occur and the effects would negate each other, requiring no compensation.

$$\mu\varepsilon = (R_1 - R_0)B + (T_1 - T_0)(C_1 - C_2) \qquad \textbf{4.1}$$

R_1 = Current reading

R_0 = Initial reading $(R_1 - R_0)$ when positive is tensile

B = Batch Gage Factor

T_1 = Current temperature

T_0 = Initial temperature

C_1 = Coefficient of expansion of steel: 12.2 microstrains/°C

C_2 = Coefficient of expansion of concrete: ~10 microstrains/°C

Since the coefficient of thermal expansion can largely vary between concrete mix designs, the Geokon method for temperature compensation was deemed by the research team as an unappealing method.

Two alternate methods were used to create a controlled environment for the field applications. Reduction of the temperature gradient through the depth of the deck as well as finding a consistent temperature to take reading provided minimal variation due to changes in temperature. While readings from the gages were recorded throughout the day

and night, readings taken at 4 am were used as the bridge would typical reach an equilibrium temperature though the height and length of the bridge and eliminate the temperature gradient. Readings were also taken around a consistent ambient temperature of 70°. This minimizes the variation between readings and keeps a consistent magnitude of influence from the temperature effects.

4.3 SH123 BRIDGE IN SAN MARCOS

4.3.1. Overview

The gages were arranged to coordinate with three different reinforcements schematics on three composite sections. In total, 12 gages were used with 4 gages in each section. Figures 4.2 and 4.3 show the layout of the gages in plan and section. Gages 1-4 monitored the additional #4 rebar bundled to the current design, gages 5-8 monitored the TxDOT standard reinforcing detail (#4's at 9 in.), and gages 9-12 monitored the additional #6 rebar bundled to the current design.

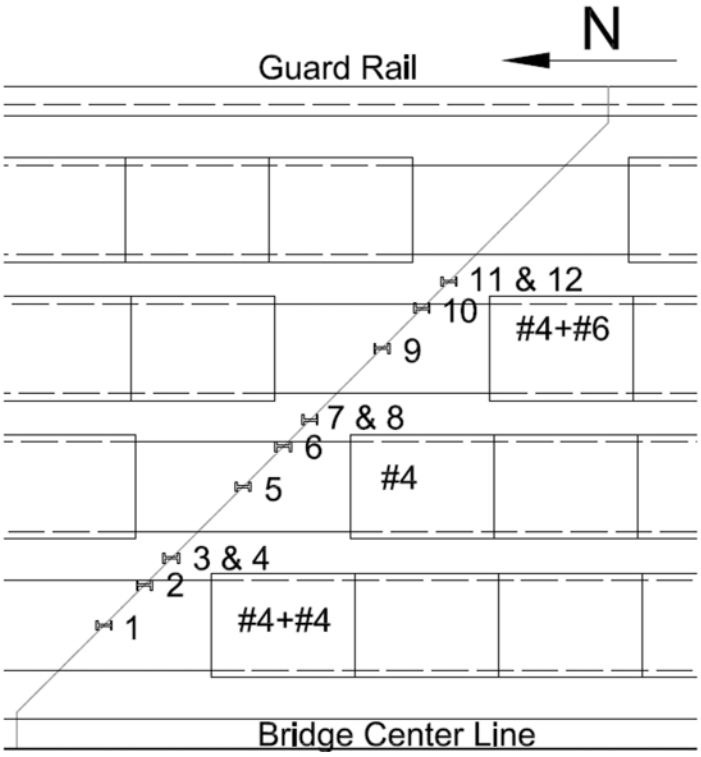

(a)

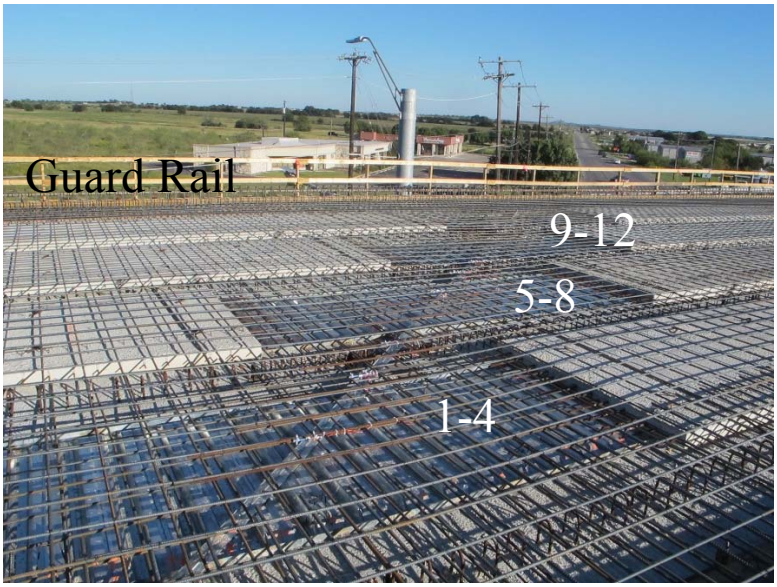

(b)

Figure 4.2 (a)-(b): Gage Layout in Plan

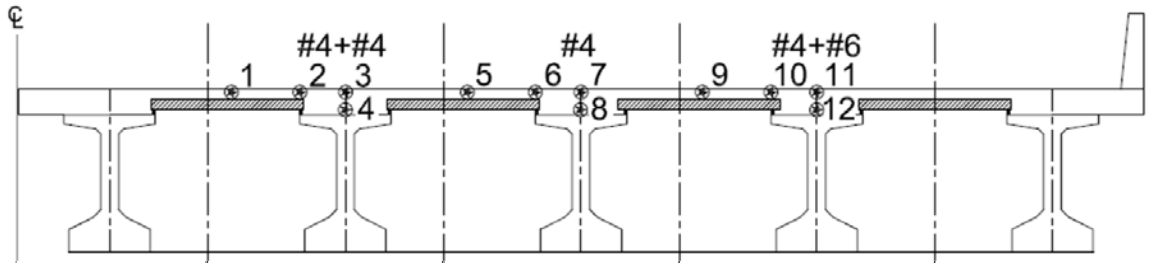

Figure 4.3: Gage Layout in Section

Some issues occurred at some of the instrumentation locations as some of the gages did not capture the strain across the crack due to the gage placement location as well as the placement of the crack former. In an attempt to capture the strain gradient through the depth of the slab, gages over the girder were placed in the top and bottom reinforcement layers. Due to the presence of a steel angle in center of the bent at the bottom of the deck, the gages were offset from the angle. As a result, this offset caused the gages 4, 7, 8, 11, and 12 to be next to the crack, as shown in Figure 4.4, rather than centered across it. Gage 10 also missed the crack. This is believed to be either from the misplacement of the gage or from the location of the zip strip placed in the top of the deck. Figure 4.5 shows which gages did not capture the strains across the crack.

Figure 4.4: Offset Gages

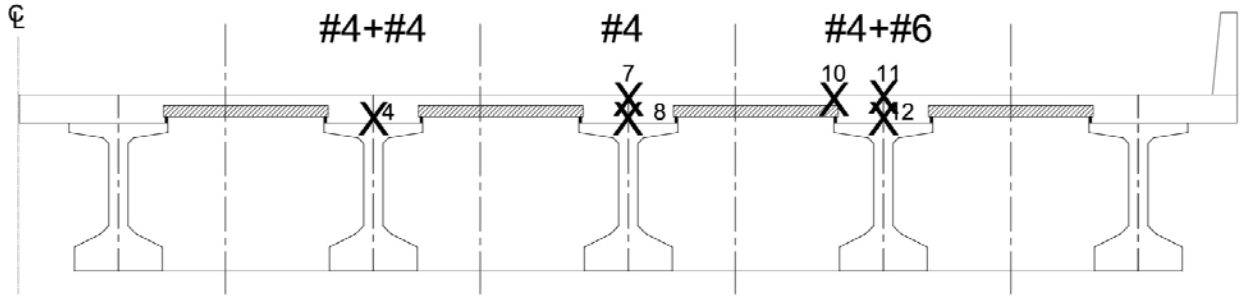

Figure 4.5: Gages Not Across Cracks

To get comparable data for each section of reinforcement, the gage centered over the panel was the only gage location to capture the crack in each case. Hence, this gage location was deemed the best indicator for the performance of the effectiveness of the reinforcement details.

4.3.2. Raw Data

The data collected from the gages is raw data and needed to be processed. Figure 4.6 shows the raw data collected from gages 1-4. Shown in the graph, the strain from gage 4 is very low, indicating the gage is not across the crack. Gages 1-3 showed trends similar to each other that fluctuate along with the average temperature in the deck. There is also an obvious distribution of strain between the middle of the panel to the girder due to the difference in stiffness and shear lag effect. The gages over the girder attract more strain.

Figure 4.6 also shows a loss of data when the battery died. The data needed to be retrieved every few days to avoid the loss of stored data when the scanning frequency was relatively high.

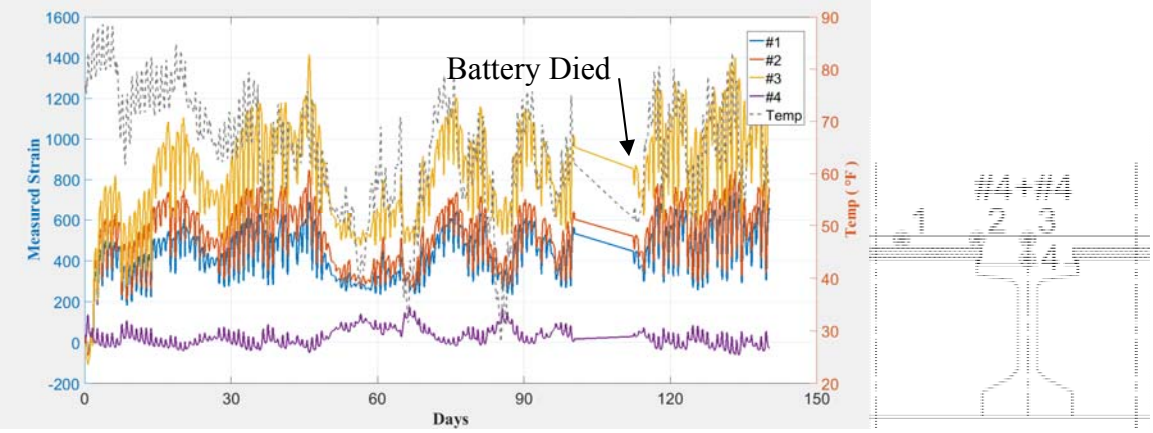

Figure 4.6: Raw Data Strains

4.3.3. Temperature Correction

As stated before, temperature fluctuations needed to be accounted for to isolate the changes in strain due to shrinkage more clearly. Reducing the temperature influence by taking readings at 4 am, when the bridge is considered to be at a temperature

equilibrium, resulted in more stable strain readings. Figures 4.7-4.9 show the strain readings from each section. The low strain values for some of the gages (i.e. gages #4, 7, 8, 10, 11, 12) clearly indicate the gages did not cross a crack.

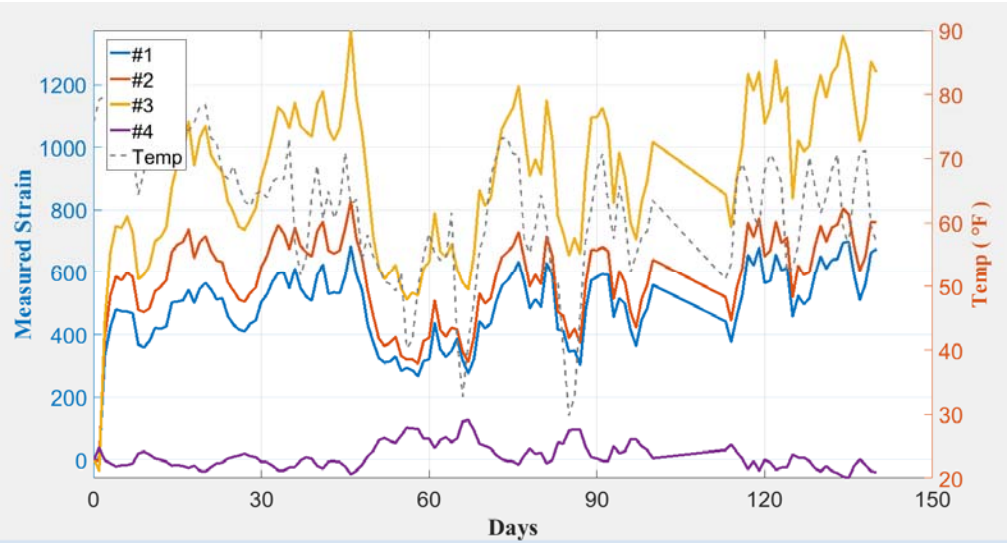

Figure 4.7: Gage 1-4 with Temperature Compensation

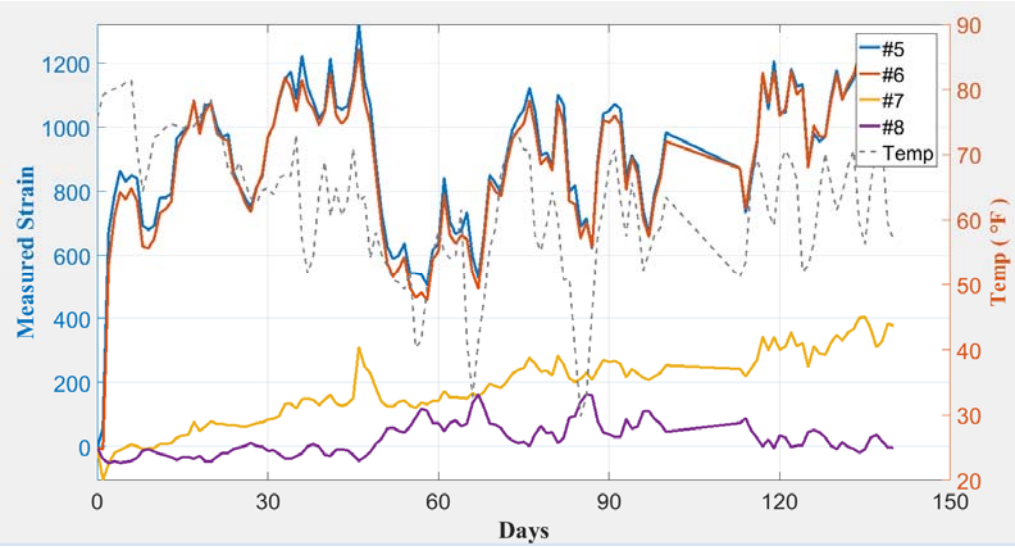

Figure 4.8: Gage 5-8 with Temperature Compensation

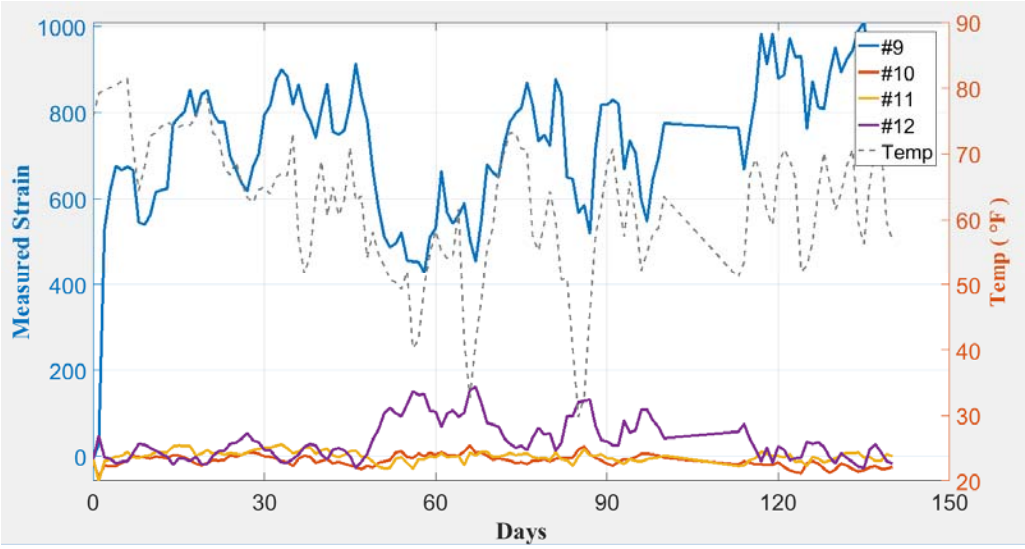

Figure 4.9: Gage 9-12 with Temperature Compensation

The gages over the panels were the most consistent gage in each section, and are the best indication of the reinforcement performance. Figure 4.10 graphs the strain values over the panel for each section. From this graph, the current design consistently has the highest strain, the additional #4 has the lowest strain, and the additional #6 is between the two. There is a trend in the reduction of strain due to the presence of steel, but it does not correlate to what was expected. The relationship between the area of steel and strain in the concrete are not directly related and account for many factors.

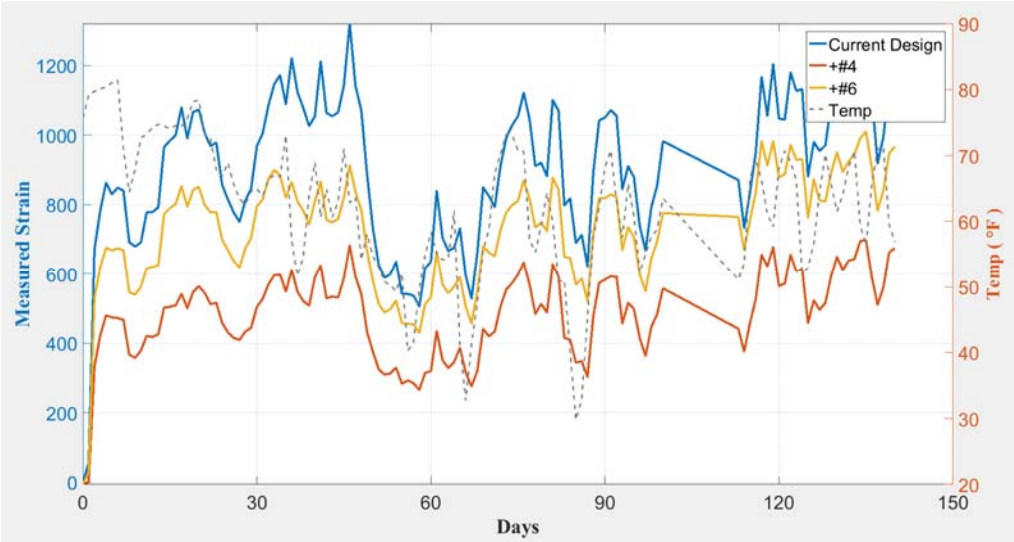

Figure 4.10: Gages1, 5, 9 over the Panels

The bottom layer gages 4, 8, and 12 all show low measured strains shown in Figure 4.11. This indicates that there may be bending within the deck and not only axial tension. Since the crack propagated from the top of the deck, it is possible that only the top half of the deck may be and the bottom half remains un-cracked.

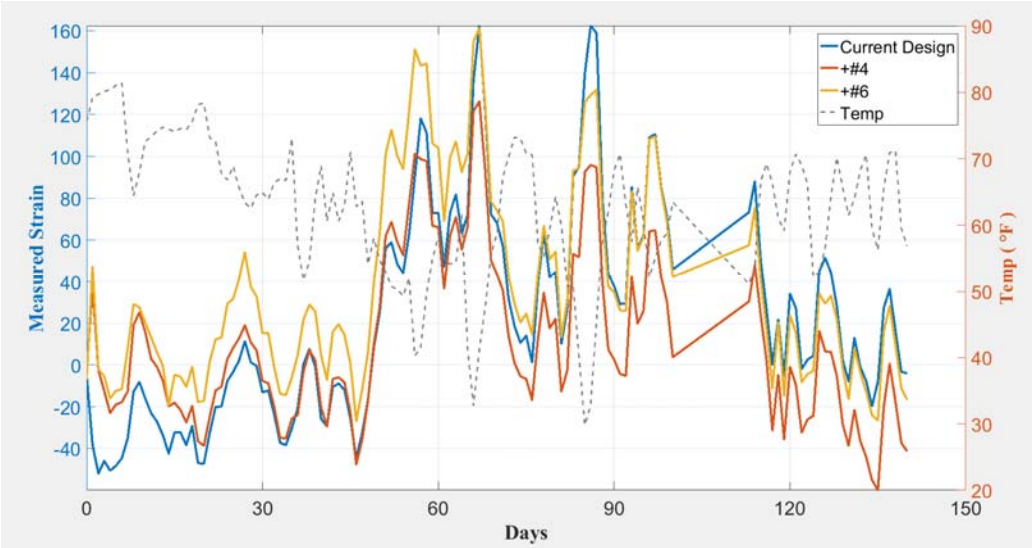

Figure 4.11: Bottom Layer Gages

4.3.4. Strain Results

The majority of the shrinkage generally occurs within the first month following the concrete placement. Figure 4.12 shows a best fit line of data collected at 70°F. This line shows a similar trend to the behavior describe in Collins and Mitchell (2007) equation for shrinkage shown in Chapter 2 equation 2.3. This graph is not intended to detail the specifics of the equation, but rather to model the behavior of the concrete in the bridge.

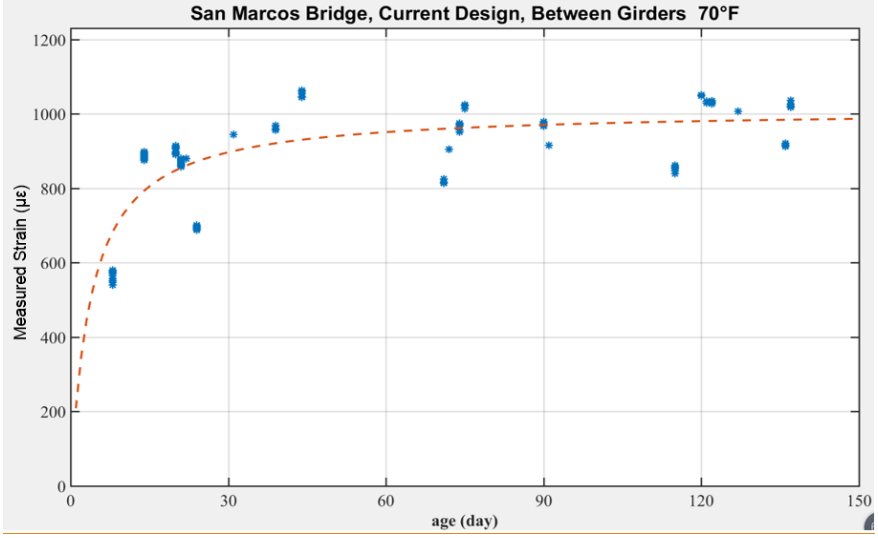

Figure 4.12: Strain Sources

4.3.5. Material Testing

Compression cylinder tests were conducted to get the strength of the concrete. In addition to getting the strength, the modulus of elasticity (E_c) was determined for the initial loading portion of the curves when the concrete stress strain relationship is relatively linear. From these material properties, the stress values can be determined from the strain value using Hooke's Law ($\sigma=E_c\varepsilon$) based on the amount of strain measured from

the gages. Split cylinder tests were used to determine the tensile strength of the concrete. Figure 4.13 shows one of the specimens following the test. The fracture in some of the aggregate indicates a high strength concrete was used for the deck. This also shows what type of aggregate was used.

Figure 4.13: Material Testing

Table 4.1: Material Strengths

Compression Strength f'c	Elastic Modulus E	Split Cylinder ft
7.5 ksi	5220 ksi	560 psi

The tensile tests provided the estimated tensile capacity of the bridge deck. The measured stress correlates to a value of $6.5 * \sqrt{f'_c}$ within the normal range for tensile strength. This correlates to a cracking strain load of 124 με.

4.3.6. Live Load Test

Live load tests were conducted to understand the influence of traffic loads. All tests were static loads with five readings taken per truck location. Chapter 3 describes in detail the truck positions for each load case. Figure 4.14 shows the average of the five recorded strain values for the load case of the truck positioned over the respective gages. From these values, based on the gages over the panels, there is a trend of reduction of strain due to the increase in the deck steel reinforcing area. The current design reinforcement had the highest strain while the additional #6 had the lowest strain as expected. The strains from the additional #6 (85με) and the additional #4 (78με) had a respective reduction of 39.6% and 47.8% in maximum strain, relative to the existing detail which had a strain of 127με.

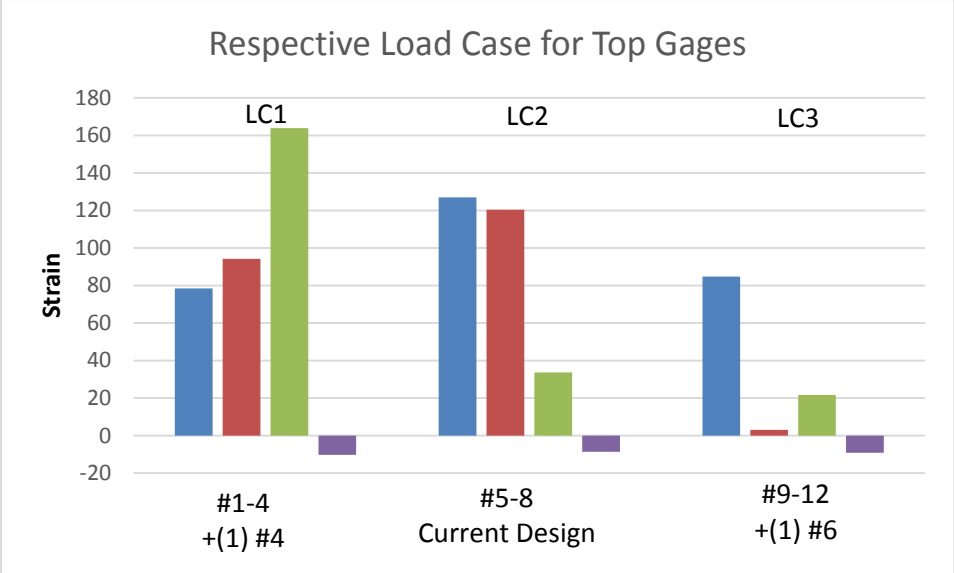

Figure 4.14: Top Layer Live Load Strains

The bottom layer gages showed compression values from the live load test. These results are small, but give an indication that there could be some bending within the concrete deck.

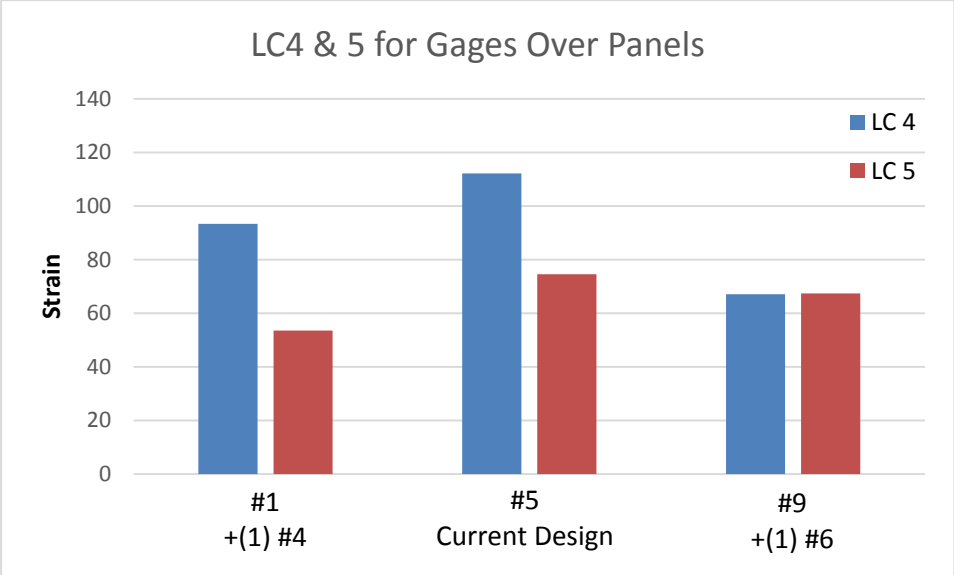

Figure 4.15: Load Case 4 with Gages Over the Panels

Load case 4 gave similar trends as the first three tests. However, load case 5 did not provide enough of a trend to make a conclusion, as shown in Figure 4.15. Hence load case 4 will be used as the primary results for the side-by-side data. The sections with additional reinforcement shower a correlation of strains lower than the current design section. The difference between the current design (112 με) and both the additional #6 (67 με) and the additional #4 (93 με) is a reduction of 50.3% and 18.6%.

Between each load case, crack formations in the top of the deck were observed and recorded. Before the test started, some cracks had already propagated from the zip strip embedded in the top of the deck. Figure 4.16 shows the extent of each crack marked with a number in the sequential order and which load case it occurred during indicated by LC. Multiple cracks elongated during a subsequent load case. Most crack origins started

at the bent cap centerline where the girders met. From there, the cracks typically propagated at a diagonal to the adjacent girder. The diagonal cracking pattern is believed to be due to the skew of the bridge. Cracks also formed near the end of the 4 ft. additional bundled reinforcement. However, this cracking may not be directly linked to the length of the reinforcement.

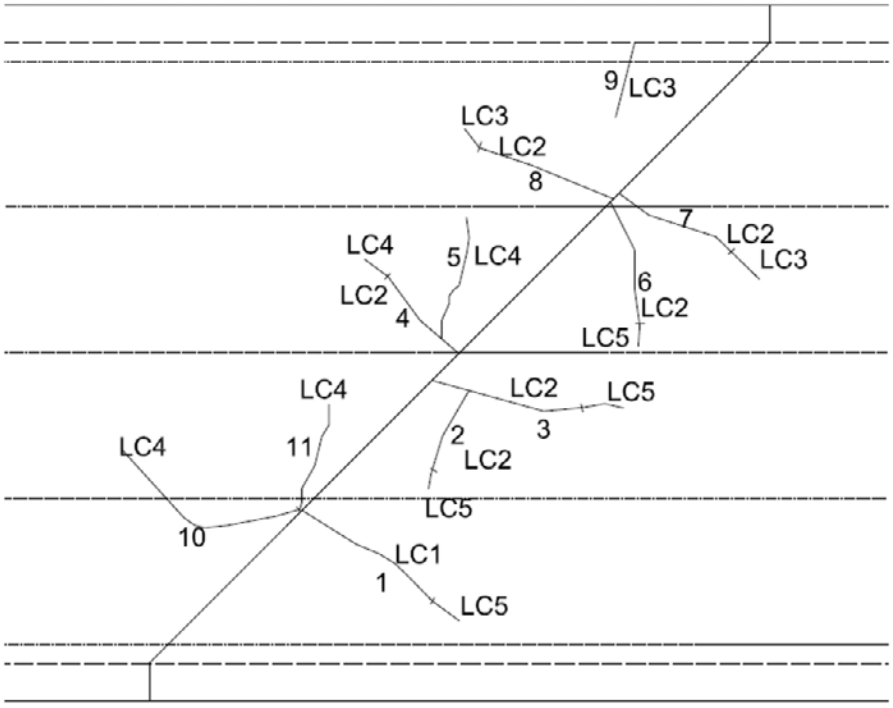

Figure 4.16: Crack Diagram

Most cracks formed with both trucks centered over a single girder. Attempts were made to measure the crack widths using a crack gauge indicator, however, the cracks were too small to be able to read with the gauge. All cracks closed after the trucks were removed.

Girder deflection readings were taken from the underside of the North span. A Hilti Laser Rangefinder was used to measure the initial and loaded height of the girder.

Three readings were taken per test. The difference between the initial and loaded heights were averaged to determine the deflection. As shown in Table 4.2, the deflections of the girders ranged from 1/16”-1/8 for most of the tests. The maximum deflection of 3/16” occurred during Load Case 4 with the trucks side by side on one span. The South span deflections were not measured due to the street being open to traffic.

The tolerance of the rangefinder is 1/16”. The deflection readings were not significant enough and too close to the tolerance to determine deflections with enough precision. Hence, the deflections were not considered for those cases.

Table 4.2: Live Load Deflections

Load Case	Girder	Average Deflection
1	2	1/8”
2	3	1/16”
3	4	1/16”
4	2	3/16”
	3	1/16”
	4	1/16”

4.4 SH71 BRIDGE IN BASTROP

4.4.1. Overview

Similar to the bridge in San Marcos, the SH71 Bridge in Bastrop used three different configurations of reinforcement as described in Chapter 3. The original reinforcement layout was intended to be identical to the San Marcos reinforcement. However, after inspection of the reinforcement and the additional steel already in place,

the layouts were changed as to not congest the concrete with steel. Figures 4.17 - 4.19 show the gage layout in plan and section views. Gages 1-4 monitor the one additional #4 rebar added to the current design, gages 5-8 monitor the current design, and gages 9-12 monitor the two additional #4 rebar added to the current design.

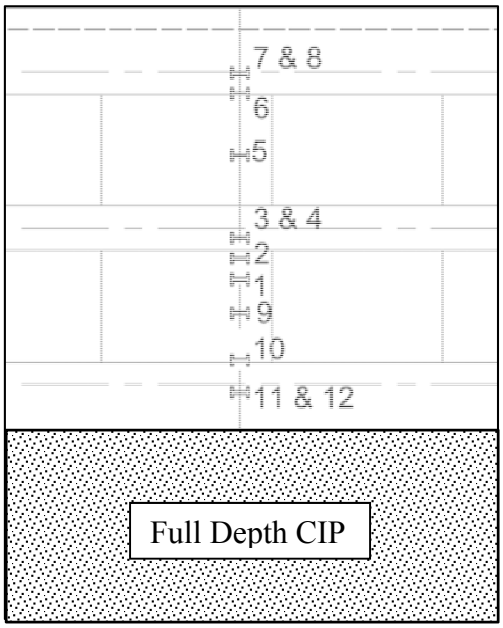

Figure 4.17: Gage Layout in Plan

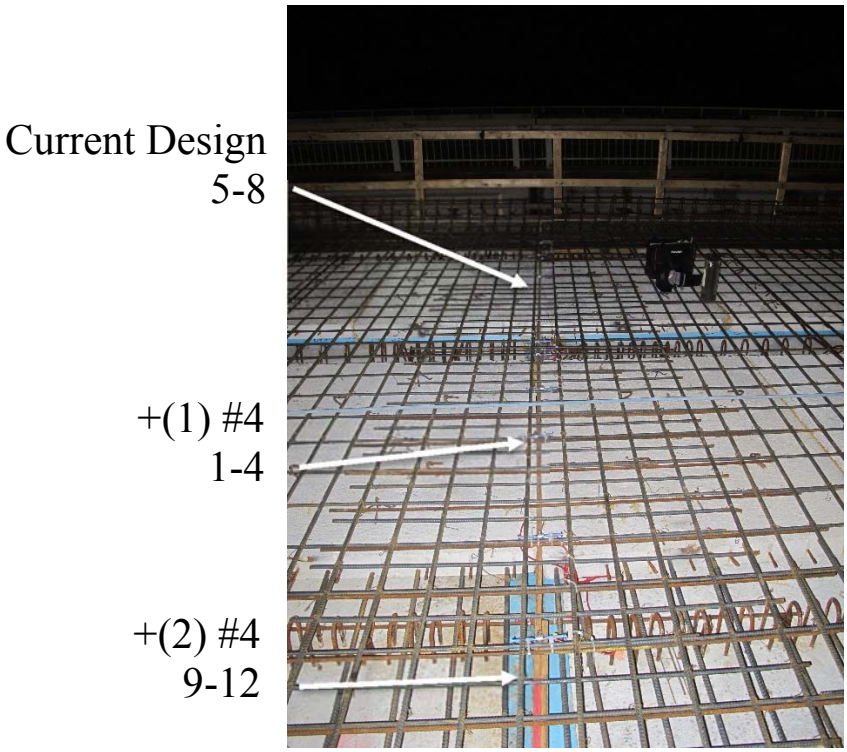

Figure 4.18: Gage Layout in Plan

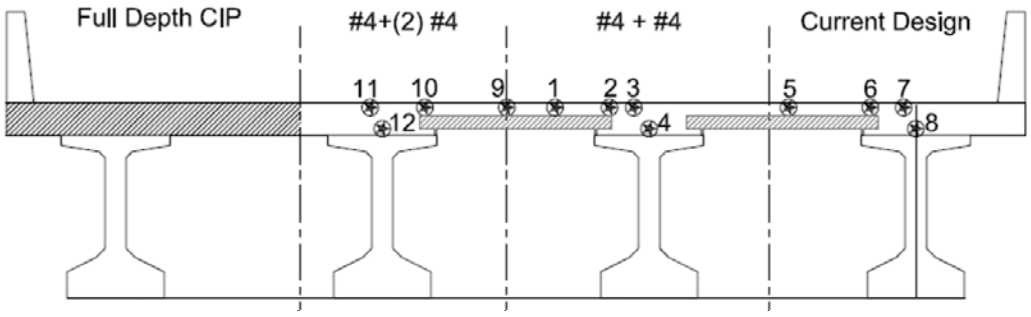

Figure 4.19: Gage Layout in Section

After issues with the placement of the gages in San Marcos, more attention was given to center the gages over the crack former to guarantee the gages captured the strain across the crack. Since the crack initiator in this bridge was located at the bottom of the deck, rather than the top, capturing the strain across the crack was more likely. To avoid the same issues of offsetting the gages over the girder as San Marcos, with permission of

the contractor, a hole was cut out in the wood crack former to place the bottom gage through. The hole ensured the gage would capture the strain from each side of the crack as shown in Figure 3.45. Doing this avoided any chances of being offset from the crack location. More details of the gages are given in Chapter 3. The top layer gages were also carefully placed directly over the crack former.

4.4.2. Raw Data

From the data collected, it is apparent that all gages are across the crack. They each show similar trends to each other and their strain values are as expected. Figures 4.20 - 4.22 show the temperature compensated strain data of the four gages from each section. In each case, the top layer gages show positive strains and the bottom layer gages typically show negative.

The standard reinforcement section girder is an exterior girder, hence a difference in stiffness and load when compared to the interior girders. The guard rail was also constructed over the exterior girder on approximately day 35. The time of construction is indicated on the graphs of gages 5-8 showing the additional strain from the weight of the barrier.

4.4.3. Strain Results

Similar to the procedures outline on the San Marcos Bridge, large fluctuations due to temperature effects were reduced by taking the gage readings at 4 am. The measured strains are more consistent and the behavior at the joint is more distinguishable. Some variations in the strain are due to additional loads on the bridge deck during construction that may change daily and are nearly impossible to quantify. The large additional load in the exterior girder was the guard rail construction around day 35. This additional load

was supported entirely by the exterior girder, causing an increase in strain. During a portion of the construction of the guard rail, the batteries died and some data was lost. Shifts in the strain only affected the exterior girder, while the two interior girders remained unaffected. The shift from before the guard rail to after it was cast was about a difference of 236με. This should be taken into account when comparing each of the three sections.

There is a distribution of strain across the width of the deck caused by the shear lag similar to that experienced in San Marcos. This consistent trend gives confidence to determining the strain distribution and where a worst case scenario may be.

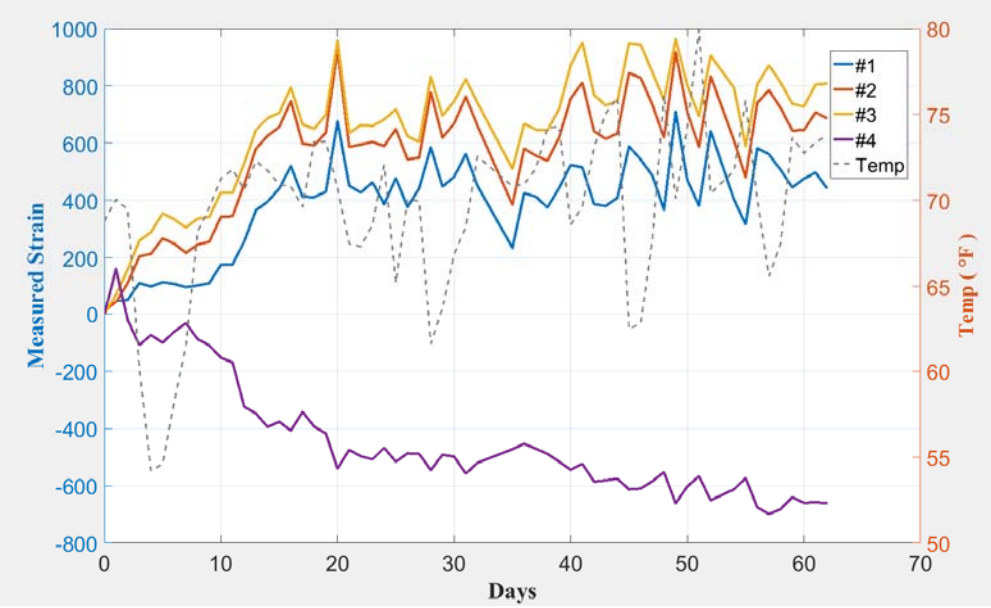

Figure 4.20: Gage 1-4 with Temperature Compensation

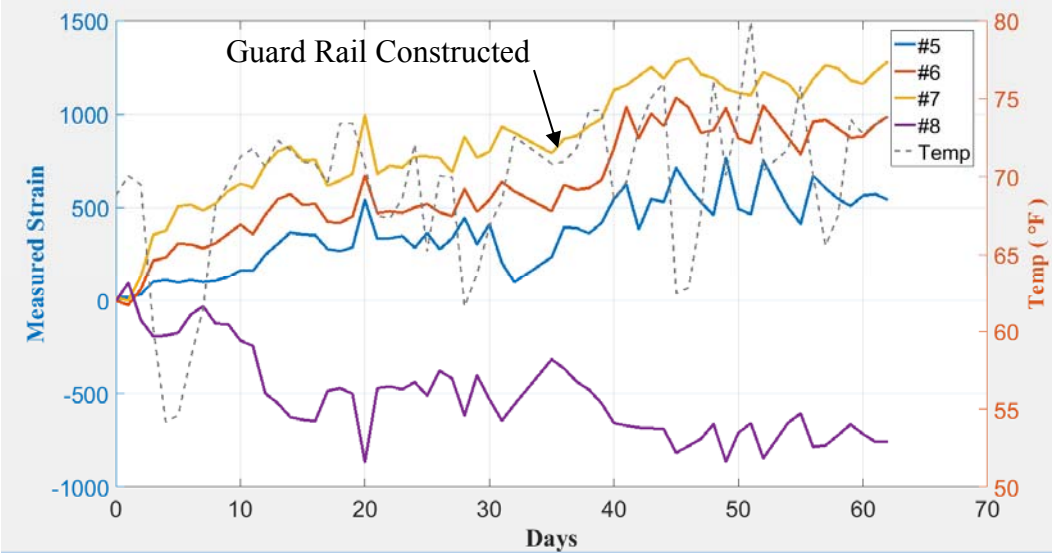

Figure 4.21: Gage 5-8 with Temperature Compensation

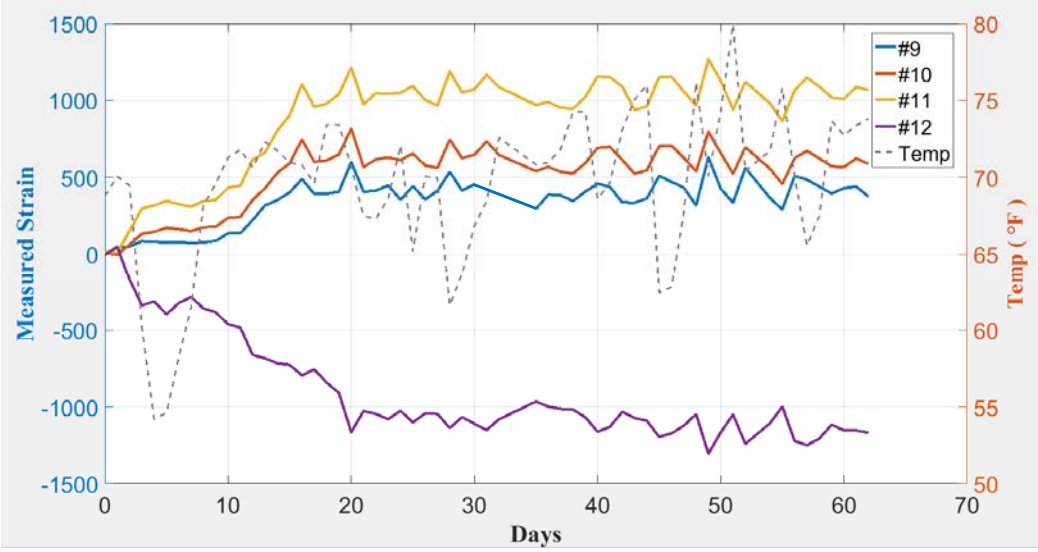

Figure 4.22: Gage 9-12 with Temperature Compensation

A comparison between similar gage locations for each section shows the influence of the steel on the measured strain. Despite the changes in areas of reinforcements, most of the strain values are relatively similar. There is not a consistent trend between the sections of adding steel to the section to reduce the strain in the

concrete. In an attempt for direct comparison, gages from similar locations are plotted together in Figures 4.23 - 4.26. Gages over the panel show the highest strains correlating to the reinforcement section with one additional #4 bar followed by the section with two #4 bars, and the standard reinforcing having the lowest strain. Gages over the girders show a different trend where the highest to lowest strains are two additional #4's, standard reinforcement, and one additional #4 respectively. The standard reinforcement and one additional #4 have very similar values.

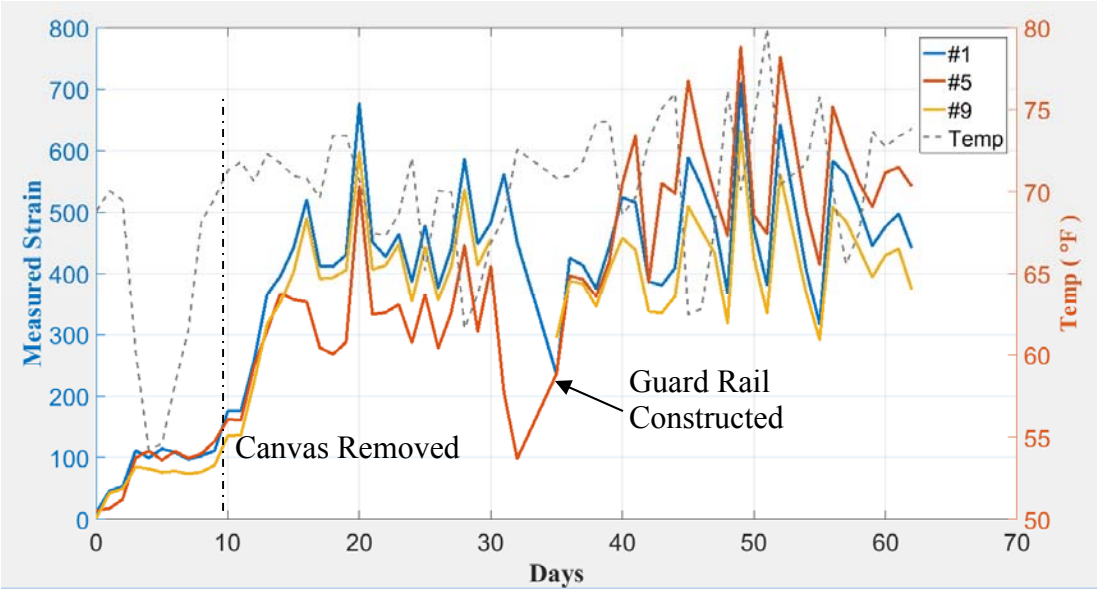

Figure 4.23: Gages 1, 5, 9 over the Panels

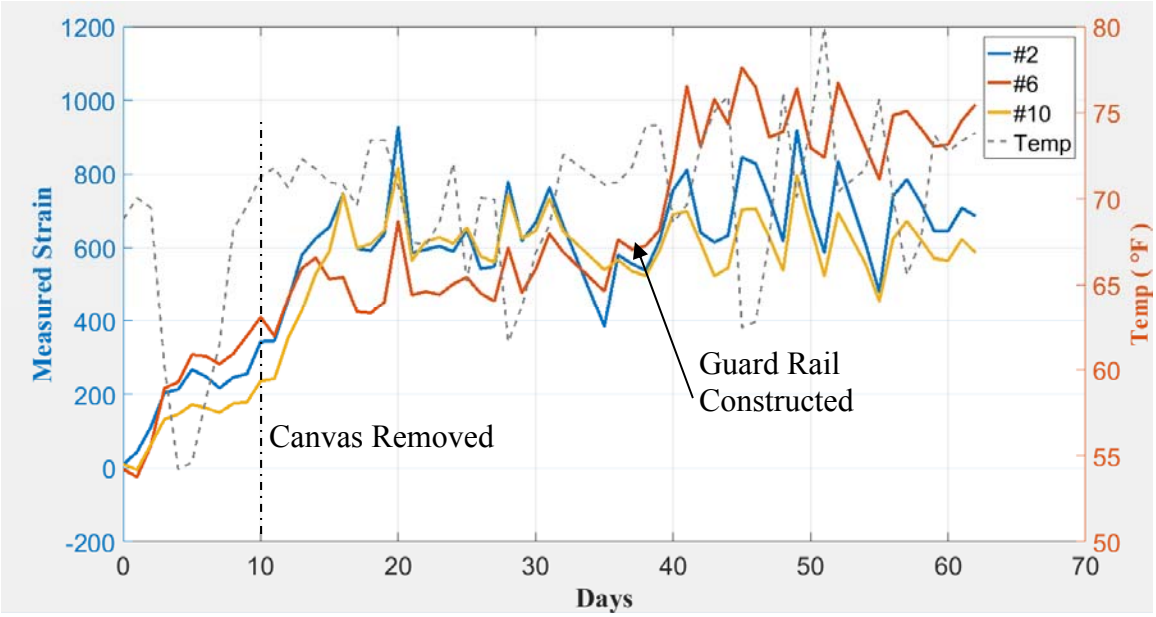

Figure 4.24: Gages 2, 6, 10 at the Edge of the Panels

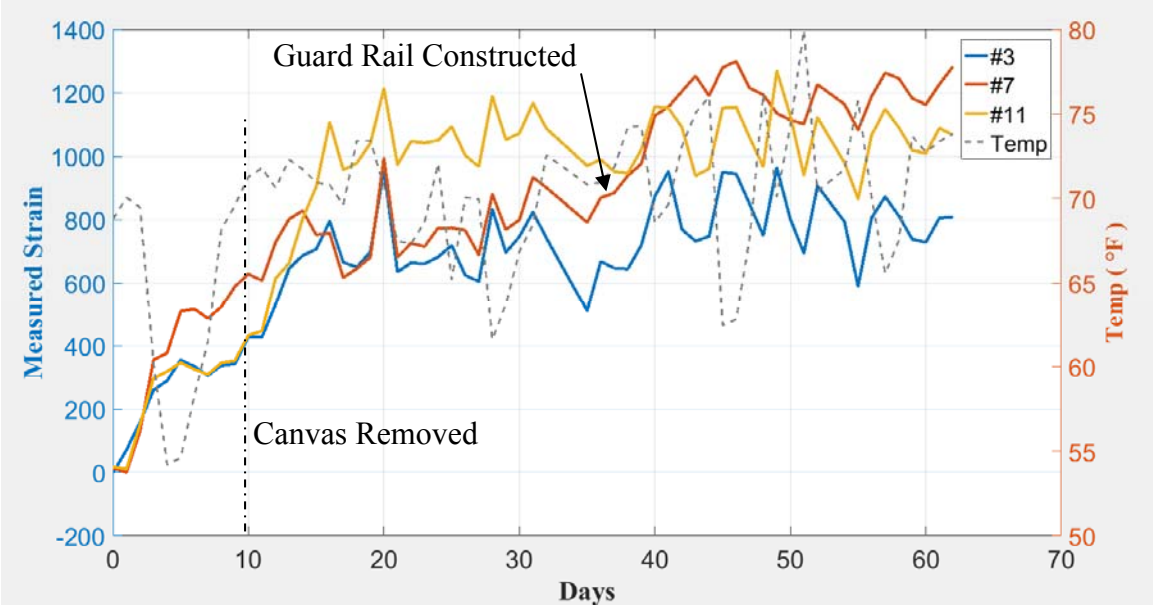

Figure 4.25: Gages 3, 7, 11 Top Layer gages over the Girder

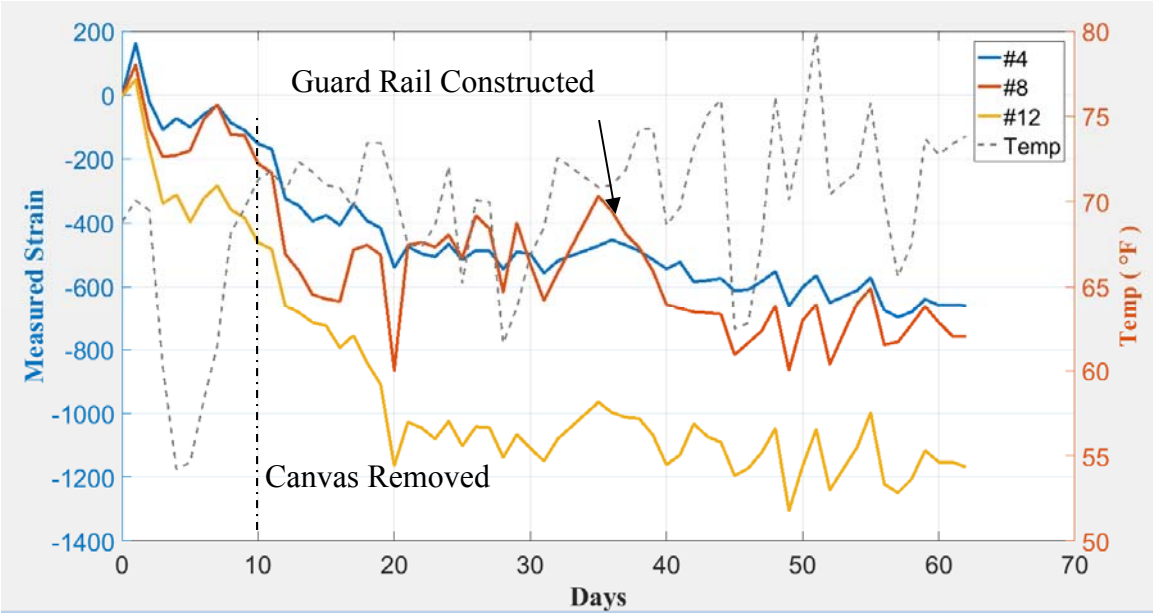

Figure 4.26: Gages 4, 8, 12 Bottom Layer Gages over the Girders

4.4.4. Material Testing

Material tests were conducted to get the strength of concrete. In addition to the tension tests performed for the San Marcos Bridge, a Modulus of Rupture Beam Test, shown in Figure 4.27, was conducted for flexural tensile capacities. Figure 4.28 shows the fractured specimen from the split cylinder tests. The fracture through the aggregate indicates a high strength concrete was used for the deck, shown in. This also shows what type of aggregate was used.

Figure 4.27: Modulus of Rupture Test

Figure 4.28: Split Cylinder Test

Table 4.3: Material Strengths

Compression Strength f'_c	Elastic Modulus E	Split Cylinder f_t	Modulus of Rupture f_r
5.1 ksi	5120 ksi	630 psi	560 psi

The strength test values shown in Table 4.3 provided the estimated tensile capacity of the bridge deck. From the Split Cylinder and the Modulus of Rupture tests, the measured tensile stresses correlate to a value of $8.8 * \sqrt{f'_c}$ and $7.8 * \sqrt{f'_c}$ which are higher than the normal range for tensile strength. This correlates to an estimated cracking strain between 109-123 με.

4.4.5. Live Load Test

Live load testing followed the same procedure as in San Marcos using five truck configurations described in detail in Chapter 3. The first three tests positioned both trucks

over one girder with one truck at mid-span of the girder on either side of the pier. The last two tests concentrically positioned both trucks side-by-side at the mid-span of either span. Truck weights were maximized to the trucks' load carrying capacity, yet were not to the service load set by AASHTO. Assuming two lanes, the un-factored service live load included the design truck load and lane load. The actual test loads were 43% of the service live load. Despite the reduction in test load, significant data was still collected.

The measured strain from the static tests shows the highest to lowest strains are the sections standard reinforcing, with one additional #4, and two additional #4's respectively as shown in Figure 4.29. However, the standard reinforcing section does have a lower strain attributed to it since the trucks were not able to be centered directly over the girder due to the guard rail. The trucks were positioned as close to the rail as feasible by the drivers. After accounting for the offset of the trucks, the standard reinforcement is expected to have higher strain values.

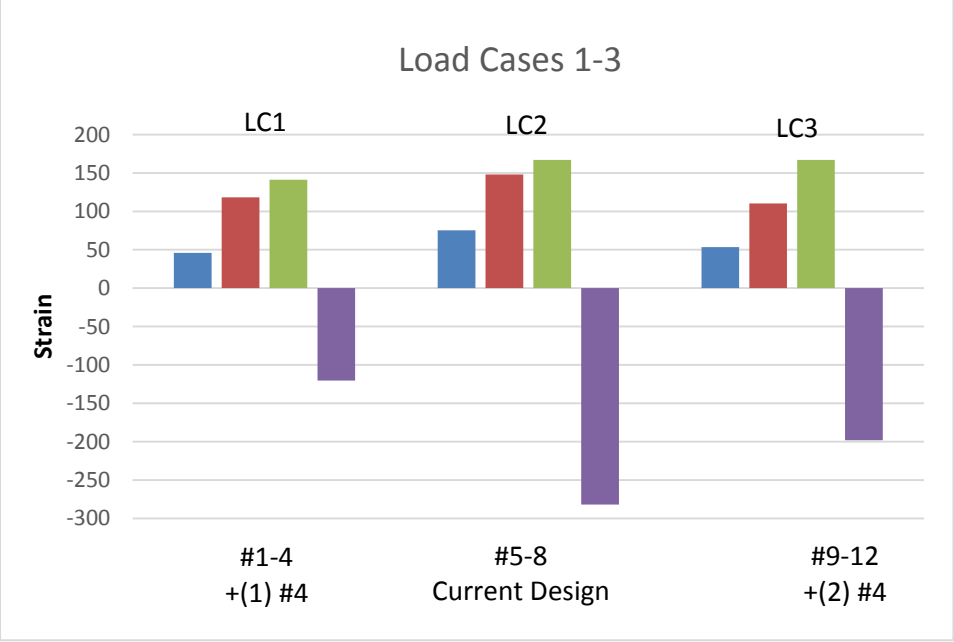

Figure 4.29: Live Load Strains

The strain through the depth of the deck also proves to be beneficial in modeling the behavior of the bridge. The bottom strains shown in Figure 4.29, depict large amounts of bending occurring within the deck.

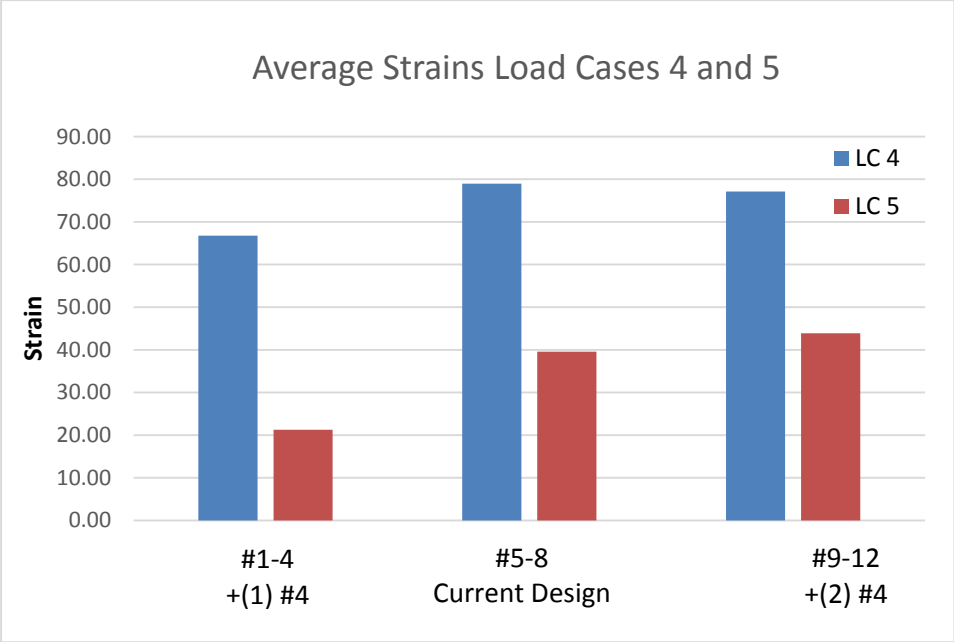

Figure 4.30: Live Load Strains

Load cases 4 and 5, shown in Figure 4.30, should have similar strain values, but give very different magnitudes of strain instead. Trends between the two load cases are still similar. This is due to unknown reasons. Nonetheless, Load Case 4 will be used as the primary results for the side-by-side test. Since all gages are across the crack, the average values of the top layer gages are used to compare the benefits to each section. This average value compares similarly to the values obtained from Load Cases 1-3.

The surface of the deck had already been textured by saw cut grooves making the visibility of cracks difficult. However, careful examination identified any cracks in the deck to be recorded before and during the live load tests. A single continuous crack propagated across the centerline of the bent before the tests started. Similar to San

Marcos, the hairline crack was hardly measureable shown in Figure 4.31. This line was traced to indicate the existing crack. During the test, no additional cracks formed.

Figure 4.31: Crack Width

Deflections from the live load tests were not significant to draw conclusions on the behavior of the bridge. Table 4.4 shows the average deflections from the tests.

Table 4.4: Live Load Deflections

Load Case	Girder	Average Deflection
1	2	3/16”
2	3	3/16”
3	4	1/4”
4	2	1/4”
	3	3/16”
	4	3/16”

4.5 SUMMARY

The results from monitoring the strains during the early stages of the bridge deck and live load testing show the influences of additional reinforcement. Adding additional steel does not have a direct correlation with the reduction of strain in the deck, however there is a relationship between the two. There are many ways to evaluate the effectiveness of steel controlling crack widths. For the purpose of this research, the control of cracking was quantified by measuring the strain in the concrete and observations of the cracks formed in the top of the deck.

Chapter 5: Conclusion

5.1 SUMMARY

The data collected in this research is to provide a measure of the performance of concrete deck reinforcing details in controlling stresses/strains over interior bents. The thesis provided an overview of field monitoring on two different bridges and also discussed the geometry of another bridge that will be monitored in late Fall 2017 or early Spring 2018. The primary focus of the thesis was the data gathered from the two instrumented bridges. The two bridges monitored provide data that compare differing bridge geometries, bridge types, and their ability to reduce stress using different reinforcing details. The timeframe of monitoring spans from the time of casting the concrete deck until the bridge is opened to traffic. Vibrating Wire Gages (VWGs) were placed at strategic locations across the deck to represent the behavior of the bridge. Within the monitoring timeframe, strains in the deck were recorded to determine the influences of shrinkage, creep, temperature and live loads.

The motivation for this study is to determine the effectiveness of the current TxDOT reinforcement standard at controlling cracks in the top of bridge decks. From this research, data from field monitoring were compiled. This data along with data from future instrumentation results will be used to develop an evaluation on the performance of the current TxDOT detail as well as making any appropriate recommendations that might improve the behavior.

5.2 BRIDGE GEOMETRY SUMMARY

A comparison between the bridges outlines the differences and similarities between the testing samples. The two monitored bridges have different geometries and

slab details over the pier. The third bridge is outlined in preparation for monitoring as well. Specific details on the bridge geometries and construction are given in Chapter 3. Bridge characteristics are summarized in Table 5.1.

Table 5.1: Bridge Geometries

	San Marcos SH123	Bastrop SH71	Round Rock IH 35
Support Condition	45° Skew	Normal Supports	Normal Supports
Girder System	Simply Supported	Simply Supported	Continuous
Deck at Joints	8 in. CIP Layer w/ PMDF	4 in. PCP + 4 in. CIP	4 in. PCP + 4.5 in. CIP
Concrete Strength	7.5 ksi	5.1 ksi	4 ksi*
Super-Structure	5 Girders	4 Girders	4 Girders
Deck Width	36 ft.	26 ft.	24 ft.
Crack Method (Location)	1.5 in. Plastic Zip Strip (Top)	7 in. Wood Crack Former (Bottom)	7 in. Wood Crack Former (Bottom)
Spans	118 ft. + 114 ft.	120 ft. + 110 ft.	180 ft. + 250 ft.
Girder Type	Tx54	Tx54	Haunch Girder
Truck Load	49.4 kips , 49.1 kips	46.3 kips , 49.5 kips	-----

**assumed value*

5.3 GAGE PERFORMANCE

The strain values for each bridge are not directly comparable, but do provide insight into the behavior of each bridge. The data collected is difficult to estimate using theoretical values due to the complexity and various restraints within the bridge structure.

Any errors in the data collection should be attributed to the gage locations in relation to the crack, various restraints inherent within the deck, and any shifting during the construction process. The gages themselves should be considered reliable.

5.4 ANALYSIS

As shown in previous sections, the performance of the varying reinforcement layouts stayed relatively consistent with each other. The crack widths in each bridge were not large enough to noticeably vary between the different sections of reinforcement. Hence, conclusions on the area of steel could not be drawn based on the crack widths. The lack of crack formations in the Bastrop Bridge could indicate benefits derived from the spacing of the reinforcement rather than the area used. The measured data did show a relationship between the amount of steel and the strain in the deck. There was not a consistent relationship however, and other variables factor into the effectiveness of the reinforcement. These will be further evaluated in future studies.

5.5 RECOMMENDATIONS

Based on the results, the current deck reinforcing detail generally performed adequately in controlling the amount of strain in the deck. Although the project is continuing, based upon the first two "poor-boy continuous" bridges that were monitored, the current size of the longitudinal bars should remain the same. The most beneficial to the controlling of cracks may be the additional intermediate bar placed between the standard longitudinal bars. This detail is standard for PCP decks and may prove beneficial to be implemented in similar decks. From observations, the current design performs adequately.

5.6 FUTURE WORK

This project will continue until 2018. Until the completion of the project, more research will be conducted using field monitoring of bridges including the continuous span bridge in Round Rock, TX, finite element modeling, and laboratory testing. Each of these will provide new insight and results.

5.7 CONCLUSION

The following conclusions are based primarily on the data collected from bridges utilizing simply supported girders with a PCP and CIP deck and poorboy joint. Field monitoring and live load testing have provided the following results for this project.

- The current reinforcement detail performs adequately
- Shrinkage contributes the highest strain in the deck
- Thermal effects vary greatly and should be accounted for
- Shrinkage strains are greater than live loads
- Increasing the reinforcement ratio did not show a direct correlation to reduction in concrete strain
- Crack formers perform differently
- Theoretical and laboratory testing will be difficult to simulate due to multiple boundary conditions and scale

References

AASHTO. (2014). “AASHTO LRFD bridge design specifications.” Washington, D.C., American Association of State Highway and Transportation Officials.

Agnew, L. S. (2007). “Evaluatoin of the Fatigue Behavior of Bridge Decks with Precast Panels at Expansion Joints”, MS Thesis, Dept. of Civil Engineering, Univ. of Texas at Austin.

Barker, J. M. (1975). Research, application, and experience with precast prestressed bridge deck panels. PCI Journal , 20 (6), 66-85.

Blok, J. (2012). "Stress Monitoring and Sweep Control Studies for Innovative Prestressed Precast Arches," Master's Thesis, The University of Texas at Austin, Austin, TX.

Broms, B. B. (1965). Crack width and crack spacing in reinforced concrete members. Journal of the American Concrete Institue , 62 (10), 1237-1255.

Buth, E., Furr, H.L., and Jones, H.L. (1972), “Evaluation of a Prestressed Panel, Cast-In-Place Concrete Bridge,” Research Report 145-3, Texas Transportation Institute, Texas A&M, University, College Station, Texas, Sept., 140 pp.

CEB-FIP Model Code (1990) : Design Code. London :T. Telford, 1993.

Chase, S., and Laman, J. (1999), “Dynamics and Field Testing of Bridges,” TRB Millenium Paper, TRB A2C05 Committee on Dynamics and Field Testing of Bridges, December, 1999. <http://onlinepubs.trb.org/Onlinepubs/millennium/00029.pdf >.

Collins, M., & Mitchell, D. (1997). Prestressed Concrete Structures. Toronto, Canada: Response Publications.

Coselli, C. J. (2004). “Behavior of Bridge Decks with Precast Panels at Expansion Joints”, MS Thesis, Dept. of Civil Engineering, Univ. of Texas at Austin.

Coselli, C. J., Griffith, E. M., Ryan, J. L., Bayrak, O., et al. (2006). Bridge Slab Behavior at Expansion Joints. Center for Transportation Research, TxDOT Research Report 0-4418-1.

Culmo, M. P. (2009). "Connection details for prefabricated bridge elements and systems" (No. FHWA-IF-09-010). < https://www.fhwa.dot.gov/bridge/ prefab/ if09010/index.cfm >

DeStefano, R. J., et al (2003). "Flexural crack control in concrete bridge structures." 3rd Proc., Int. Sym. on High Performance Concrete (ISHPC).

Dowell, R. K., and Smith, J. W. (2006). Structural Tests of Precast, Prestressed Concrete Deck Panels for California Freeway Bridges. PCI Journal, March-April, 2-13.

Foster, S. W. (2010), "Reducing Top Mat Reinforcement in Bridge Decks," Master Thesis, The University of Texas at Austin.

Frosch, R. J. (1999). "Another Look at Cracking and Crack Control in Reinforced Concrete," ACI Structural Journal, May-June, pp. 437 – 442.

Frosch, R. J. (2001). "Flexural Crack Control in Reinforced Concrete," Design and Construction Practices to Mitigate Cracking, SP 204, American Concrete Institute, Farmington Hills, Mich., pp. 135-154.

Furr, Howard L., et al (1970). "A Study of Prestressed Panels and Composite Action in Concrete Bridges Made of Prestressed Beams, Pre-stressed Sub-Deck Panels, and Cast-in-Place Deck." Four Research Reports, Project 145.

Geokon Vibrating Strain Wire Gage Instruction Manual. (2016), < http://www.geokon.com/content/ manuals/4000_Strain_Gage.pdf>

Gergely, P., and Lutz, L. A. (1968) "Maximum Crack Width in Reinforced Concrete Flexural Members," Causes, Mechanism, and Control of Cracking in Concrete, SP-20, American Concrete Institute, Farmington Hills, Mich, pp. 87–117.

Graddy, J. C., Burns, N. H., and Klingner, R. E. (1995). Factors affecting the design thickness of bridge slabs (Master's thesis, University of Texas at Austin).

Holt, John and Smith, Amy. (2014). “Reducing Steel in Bridge Decks” Concrete Bridge Views, Issue 78, Sept/Oct.

Kaar, P. H., and Mattock, A. H. (1962). "High-Strength Bars as Concrete Reinforcement —Part 4: Control of Cracking," Journal, PCA Research and Development Laboratories, V. 4, No. 1, January, pp. 46-65.

Krauss, P. D., & Rogalla, E. A. (1996). NCHRP Report 380: Transverse Cracking in Newly Constructed Bridge Decks. Washington, D.C.: National Academy Press.

Kwon, Ki Yeon. (2012), "Design recommendations for CIP-PCP bridge decks", Ph.D Dissertation, Dept. of Civil Engineering, Univ. of Texas at Austin.

Ley, T., Ghashgesh, M, and Patil, S. (2010); “Investigations of a Precast Bridge Deck System”, Report No. OTCREOS7.1-31, Oklahoma Transportation Center.

Mander, J. and Head, M. (2010), “Experimental Performance of Full-Depth Precast, Prestressed Concrete Overhang, Bridge Deck Panels”, ASCE Journal of Bridge Engineering, September/October 2010, Vol. 15, No. 5. Pp. 503-510.

Merrill (2002): Merrill, B. D., “Texas' Use of Precast Concrete Stay-In-Place Forms for Bridge Decks,” Proceedings, Concrete Bridge Conference, National Concrete Bridge Council, Skokie, IL.

NCHRP (2004), “Concrete Bridge Deck Performance: A Synthesis of Highway Practice,”Synthesis 333, National Cooperative Highway Research Program, Transportation Research Board, Washington, D.C., <*http://onlinepubs.trb.org/Onlinepubs/nchrp/nchrp_syn_333.pdf*>

Phares, B., Greimann, L., Jayathilaka, S., (2015), "Investigation of Negative Moment Reinforcing in Bridge Decks", Research Report IHRB Project TR-660, Iowa State University.

Tsui, C. K., Burns, N. H., and Klingner, R. (1986). "Behavior of Ontario-Type Bridge Deck on Steel Girders: Negative Moment Region and Load Capacity", TxDOT Sponsored Research Study 3-5-83-350, January, Center for Transportation Research, University of Texas at Austin.

Yousefpour, H. (2015) "Short-Term and Time-Dependent Stresses in Precast Network Arches", PhD Dissertation, The University of Texas at Austin.